Ore Geology Reviews 91 (2017) 928–944

Contents lists available at ScienceDirect

Ore Geology Reviews

journal homepage: www.elsevier.com/locate/oregeorev

Sulfur and lead isotope systematics: Implications for the genesis of the Riópar Zn-(Fe-Pb) carbonate-hosted deposit (Prebetic Zone, SE Spain)

Dídac Navarro-Ciurana[a,*], Esteve Cardellach[a], Elena Vindel[b], Albert Griera[a], David Gómez-Gras[a], Mercè Corbella[a]

[a] Departament de Geologia, Facultat de Ciències, Universitat Autònoma de Barcelona, Edifici Cs s/n, 08193 Bellaterra (Cerdanyola del Vallès), Spain
[b] Departamento de Cristalografía y Mineralogía, Facultad de Ciencias Geológicas, Universidad Complutense de Madrid, c/José Antonio Novais s/n, 28040 Madrid, Spain

ARTICLE INFO

Keywords:
S and Pb isotopes
Carbonate-hosted Zn-(Fe-Pb) ores
Riópar
Prebetic
Southeast Spain

ABSTRACT

The Zn-(Fe-Pb) deposits of the Riópar area (Prebetic Zone, SE Spain) are hosted by dolostones that replace Berriasian to Valanginian (Upper Jurassic-Lower Cretaceous) limestones. Mineralization consists of hypogene sphalerite, marcasite and galena, and supergene calamine zones. The hypogene ores are associated with a saddle dolomite gangue. The ore bodies occur as discordant and stratiform lenses, ore-cemented breccias, cm- to mm-wide veins and veinlets, disseminations and stylolite porosity filling within the host dolomites. The main ore controls include stratigraphy and/or lithology, tectonics (faults, fractures and breccias) and availability of metals and sulfur. The morphologies and epigenetic character of the hypogene ore bodies are consistent with the classification of this mineralization as a Mississippi Valley-type (MVT) deposit. The Ga/Ge geothermometer in sphalerite yielded a temperature range of 194–252 °C, which represents the temperature of the source region of the ore solution. This value is comparable to the temperature obtained in the ore deposition site, 159 ± 15 °C from the $\Delta^{34}S$ geothermometer in sphalerite galena pairs. This similitude points to a hydrothermal fluid that did not cool down significantly during flow from the fluid reservoir area to the precipitation site. $\delta^{34}S$ values of base-metal sulfides (−7.5 to +3.5‰) are consistent with thermochemical reduction of Triassic sulfate (seawater and/or derived from dissolution of evaporites) by interaction with organic compounds (e.g., hydrocarbons, methane), which reduced sulfate to sulfide in the deposition site. The lead isotope ratios ($^{206}Pb/^{204}Pb$ = 18.736–18.762; $^{207}Pb/^{204}Pb$ = 15.629–15.660; $^{208}Pb/^{204}Pb$ = 38.496–38.595) of galena suggest that Pb, and probably other metals as Zn, is derived from continental crustal rocks. On the other hand, these relations points to a unique metal source probably derived from the Paleozoic basement rocks. The relationship between bedding-parallel stylolites, dolomitization, sulfide precipitation and Alpine tectonic affecting the MVT ore, suggests a relative timing range for the mineralization in the Riópar area of 95–20 Ma (Upper Cretaceous-Tertiary). The sulfide mineralization and the associated dolomitization are thus explained by the contribution of two fluids that mixed in different proportions during dolomitization and mineralization: i) a fluid probably derived from Cretaceous seawater saturating Mesozoic sediments (Fluid A), characterized by being dilute and initially low temperature, which should have contained organic rich compounds in the ore deposition site (e.g., hydrocarbons and CH_4 dissolved gas); and ii) a high salinity hydrothermal brine (Fluid B) rich in both metals and sulfate, circulated through the Paleozoic basement. During the pre-ore dolomitizing stage the fluid phase was dominated by the diluted fluid (Fluid A > Fluid B), whereas in a later fluid pulse, the proportion of the high salinity fluid increased (Fluid A < Fluid B) which allowed sulfide precipitation. MVT exploration in the Prebetic Zone should focus towards the SW of the Riópar mines, in the vicinity of the Alto Guadalquivir-San Jorge fault.

1. Introduction

In the Iberian Peninsula, Zn-Pb mineralizations located within Mesozoic basins and hosted in Lower Cretaceous age carbonates were exhaustively investigated during the last decades (e.g., Fenoll Hach-Alí, 1987; Grandia, 2000; Grandia et al., 2003a,b; Perona et al., 2007; Piqué et al., 2009; Simon et al., 1999; Velasco et al., 1996, 2003). The most important districts are found in the Basque-Cantabrian Basin (N Spain), which includes the world-class deposit of Reocín (Santander), that contained reserves of over 60 Mt with ore grades up to 8% Zn and 1.5%

* Corresponding author.
E-mail address: didac.navarro.ciurana@gmail.com (D. Navarro-Ciurana).

http://dx.doi.org/10.1016/j.oregeorev.2017.08.013
Received 6 March 2017; Received in revised form 3 August 2017; Accepted 7 August 2017
Available online 17 August 2017

Pb (Velasco et al., 2000). Other deposits occur in the Maestrat Basin (Teruel-Castelló, E Spain), with Resurrección mine in the Penyagolosa Sub-Basin, estimated to contain around 30,000 t with 6.7% Zn and 0.2% Pb (Grandia et al., 2003a; Michel, 1974).

Similar Zn mineralizations occur near the Riópar village (Albacete, SE Spain), which is located in the Prebetic Zone of the Betic ranges. The first brass factory in the Iberian Peninsula and the second in Europe was erected in Riópar in the late XVIII century ("Reales Fábricas de Alcaraz"), using the oxidized parts of the Zn-(Fe-Pb) bodies. The estimated minimum Zn production was of 20,000 t (Navarro-Ciurana et al., 2016c), although the ore extraction from these mines was very irregular over the years. An exploration program, carried out by *Exploración Minera Internacional (España), S.A.* in 1972, recorded mean ore grades around 4% Zn along 257 m of mineralized old galleries (Urbano-Vicente, 1972). Furthermore, 35 surface geochemistry lines with N-S direction were prospected along 10 km to the E of Riópar obtaining Zn anomalies with a threshold of 110 ppm and exceptionally recording maximum values of 330 ppm of Zn (Urbano-Vicente, 1972). Although the known mineralization is of reduced tonnage, its study could shed light on the mining exploration potential in the Prebetic Zone, where the mines of Riópar are the only ones discovered.

No further works were performed in the area until 2001, when Grandia et al. (2001) studied the petrography of dolomites associated with the Zn mineralization, suggesting that the ore characteristics are consistent with a Mississippi Valley-type (MVT) deposit. More recent research in the area provided new petrographical and geochemical data of the host dolomites and the supergene non-sulfide Zn deposits (Navarro-Ciurana et al., 2016a,c). Mapping and stratigraphic studies revealed two stratabound dolostone bodies connected by other patchy bodies, which replace carbonate units of Upper Jurassic to Lower Cretaceous ages. The composition, temperature, origin and evolution of the dolomitizing fluid were concluded to be a brine of hydrothermal origin, which interacted with the carbonate host at temperatures between 150 and 250 °C.

The objective of this study was to define the processes that control metal precipitation in the Riópar area. More specifically, temperature, sulfur and metal sources as well as timing will be addressed, integrating geological, mineralogical, textural and geochemical data. Finally, a conceptual genetic model is proposed on the basis of these evidences and previously published data, and mining exploration targets in the Prebetic Zone are suggested.

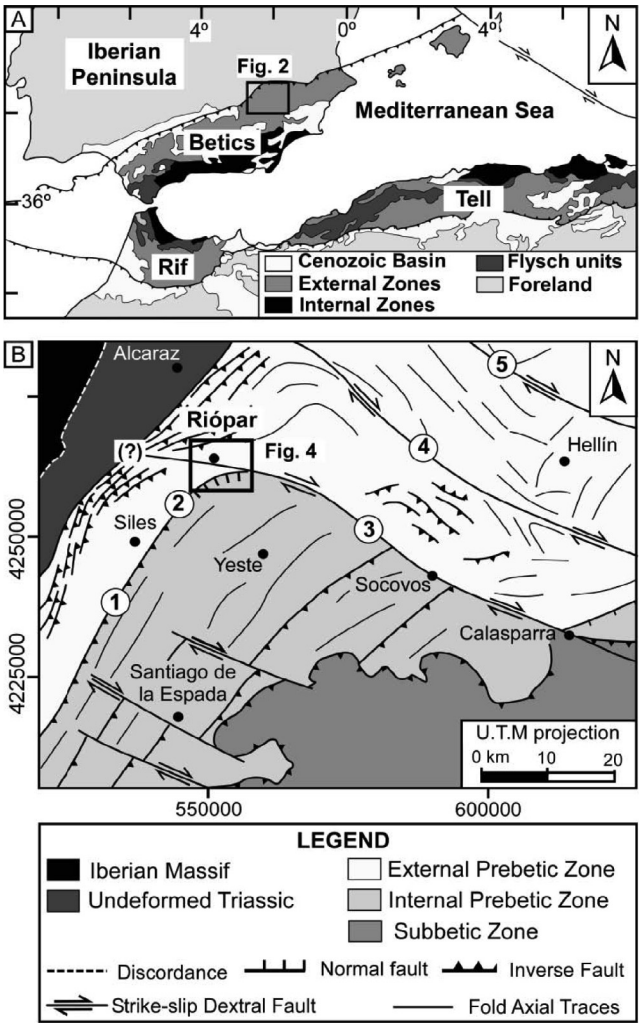

Fig. 1. A) Location of the studied area in the Betic Cordillera, SE Iberian Peninsula. Modified from Comas et al. (1999). B) Tectonic sketch with main units of the Prebetic Zone (Betic Cordillera) modified from Pérez-Valera et al. (2010) (see Fig. 3a for a general geological map of the studied area). Numbers in circles refer to: (1) Alto Guadalquivir fault; (2) San Jorge Fault; (3) Socovos-Calasparra fault; (4) Liétor fault; and (5) Pozohondo fault.

2. Geological setting

The studied area is located in the External Zones of the Betic Cordillera, which constitutes the westernmost part of the Mediterranean Alpine chain, together with the Rif in northern Morocco and Tell-Kabylies Ranges in northern Algeria (e.g., Sanz de Galdeano, 1990; Fig. 1a). The External Zones, generally subdivided into the Prebetic and Subbetic (Fig. 1b), are defined as a NNW-verging fold-and-thrust belt of the Betic orogen, consisting of Mesozoic to Cenozoic marine sediments, originally deposited in the southern part of the Iberian continental paleomargin (e.g., García-Hernández et al., 1980; Sanz de Galdeano, 1990; Vera et al., 2004).

The Riópar old mining area is located between the External and Internal Prebetic Zones (Fig. 1b), in the outer portion of the Mesozoic Betic basin. The Prebetic Zones consist of a Mesozoic and Tertiary sedimentary sequence (≤2000 m thick), which folded and detached from the Paleozoic substratum along Triassic sediments (Barbero and López-Garrido, 2006; Vilas et al., 2001). The External Prebetic Zone (Fig. 1b) is dominated by shallow internal platform facies and corresponds to the deformed part of the northern basin. This zone contains well exposed Triassic and Jurassic rocks and less Cretaceous and Paleogene sediments. On the other hand, the Internal Prebetic Zone (Fig. 1b), which is located basinwards or to the South, is dominated by marginal platform to slope facies and large folds and thrusts structures with none Triassic rocks, some Jurassic strata and extensively exposed Cretaceous and Paleogene sediments (e.g., Azéma, 1977; Barbero and López-Garrido, 2006; García-Hernández et al., 1980).

The Prebetic tectonic structure consists of a set of NE-SW trending and SE dipping faults and NW-SE trending strike-slip dextral faults perpendicular to the arc fold axes (Rodríguez-Estrella, 1979; Fig. 1b). The NE-SW trending Alto Guadalquivir-San Jorge and NW-SE trending Socovos-Calasparra faults are thought to separate the External (to the S) from the Internal (to the N) zones (Fig. 1b). The northern margin of the Prebetic zone (i.e., External Prebetic) consists of an imbricate reverse-fault structure with narrow overturned folds, overthrusting towards the central plateau ("Meseta") of Spain (N and NW), whereas the southern margin of the Prebetic zone (i.e., Internal Prebetic) shows a gentler fold and fault structure, which is overthrusted by Subbetic nappes (García-Hernández et al., 1980; Fig. 1b).

Successive tectonic periods controlled the sedimentation, which has been differentiated into four megasequence stages during the Mesozoic in the South Iberian paleomargin (e.g., Banks and Warburton, 1991; Barbero and López-Garrido, 2006; De Ruig, 1992; Vera, 2001) (Fig. 2): i) a Triassic rifting stage (Late Permian-Rhaetian), represented by the deposition of the "Germanic" facies (Buntsandstein, Muschelkalk, and Keuper); ii) an Early-Middle Jurassic post-rifting stage, characterized by

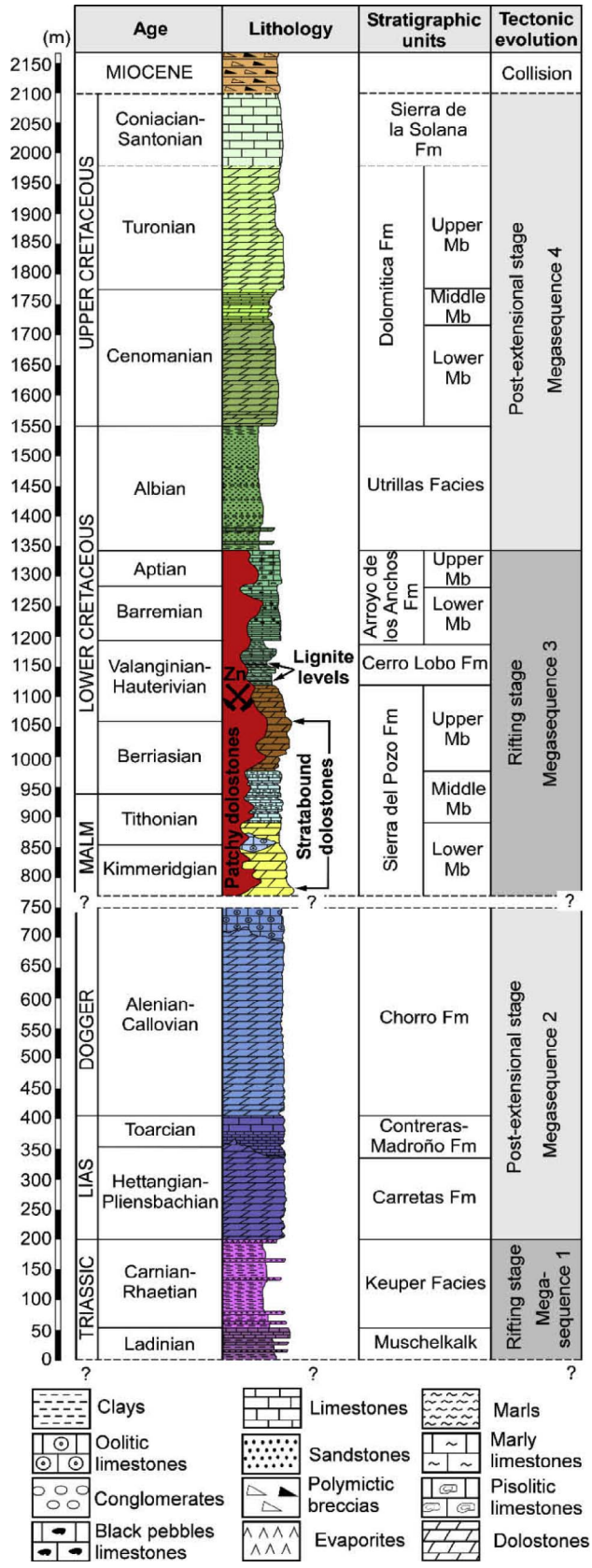

Fig. 2. Stratigraphic column of the Riópar area with sedimentary units and sequences, location of the hydrothermal dolomite bodies and Zn-(Fe-Pb) ores and tectonic evolution of the Prebetic Zone. Modified from Navarro-Ciurana et al. (2016a).

regional thermal subsidence, little fault activity and development of broad carbonate platforms; iii) a Late Jurassic-Early Cretaceous rifting cycle, which led to the separation of the Prebetic domain from the rest of the Betic basin and also from the rest of the Iberian Plate; and iv) a Late Cretaceous post-extensional thermal subsidence stage, with little tectonism and development of extensive shallow-marine carbonate platforms. The destruction of the Prebetic margin was due to the development of the Betic Chain; it started in Paleogene times, although the main collision event occurred during the Miocene (Fig. 2) as a consequence of the convergence of the African and Iberian plates (Barbero and López-Garrido, 2006).

3. Sampling and analytical methods

Systematic sampling was performed across the different dolomite bodies as well as from underground workings, dumps and surface outcrops from all mineralized areas. Sampling of all lithotypes was carried out according to spatial criteria. This was easy in surface outcrops and particularly difficult inside mines.

A total of 145 polished thin sections of dolomites and Zn-Pb-Fe sulfide ores were studied in detail using transmitted and reflected light petrographic microscopy at the *Departament de Geologia* of the *Universitat Autònoma de Barcelona* (*UAB*). Preliminary petrographic studies of thin sections were carried out at low-magnification using polarizing filters and a transparency scanner with high-resolution digital image capture. Representative polished thin sections were investigated using a Zeiss EVO MA 10 Scanning Electron Microscope (SEM) with accelerating voltage of 20 kV at the *Servei de Microscopia* of the *UAB*. The identification of different mineral phases was performed by qualitative analyses using an Energy-Dispersive Spectrometer (EDS) with a medium count time of 30 s per analysis.

The analysis of Zn-Fe-Pb sulfides were performed using a five-channel JEOL JXA 8900 Electron Microprobe (EMP) at *ITCS Centro Nacional de Microscopía Electrónica* of the *Universidad Complutense de Madrid* (*UCM*). The analytical conditions were: 20 kV accelerating voltage, 50 nA beam current, 5 μm beam diameter and counting time of 20 s per element. Calibrations were performed using natural and synthetic standards. Standards, diffracting crystals and analytical lines were as follows: galena (S, PETH, Kα; and Pb, PETH, Mα), Fe metal (Fe: LIF, Kα), sphalerite (Zn, LIF, Kα), Cd metal (Cd, PETJ, Lα), Bi metal (Bi, PETJ, Mα), GaSb (Sb, PETJ, Lα), Sn metal (Sn, PETJ, Lα), GaAs (Ga, TAP, Lα), Rb glass (Ge, TAP, Lα), MnO_2 (Mn, LIF, Kα), Ag metal (Ag, PETH, Lα), Ni metal (Ni, LIFH, Kα), Co metal (Co, LITH, Kα), Cu metal (Cu, LIF, Kα). LIF, PET and TAP are the diffracting crystals detected element wavelengths for each mineral phase, whereas large area and high intensity PET crystals are indicated with an H and L, respectively.

Sphalerite, marcasite and galena were separated by hand picking under a stereomicroscope for sulfur isotope analyses. These were performed at the *Centres Científics i Tecnològics* (*CCiTUB*) of the *Universitat de Barcelona* (*UB*), using a Delta C Finnigan MAT Delta-S isotope ratio mass spectrometer (IRMS), with a precision better than ± 0.1 per mil. The isotope ratios were calculated using the NBS127, IAEAS1, and IAEAS3 standards and reported relative to the Vienna-Canyon Diablo Troilite (V-CDT) standard.

Lead isotope compositions were determined on hand picked galena under a stereomicroscope. Ten mg of sample powder were dissolved in 100 μL of HNO_3 65%. The lead aliquots were extracted using the centrifugal separation method and loaded on single Re-filaments with 1 μL of 1 M H_3PO_4 and 2 μL of silica gel. The $^{206}Pb/^{204}Pb$, $^{207}Pb/^{204}Pb$ and $^{208}Pb/^{204}Pb$ isotopic ratios were performed at the *Centros de Apoyo a la Investigación* (*CAI*) of the *UCM*, using a Thermal Ionization Mass Spectrometer TIMS-Phoenix at 1400 °C. The Pb isotope composition was corrected for mass fractionation calculated from replicate measurements of the NBS-981 standard ($^{206}Pb/^{204}Pb = 16.899 \pm 0.223\%$, $^{207}Pb/^{204}Pb = 15.441 \pm 0.323\%$ and $^{208}Pb/^{204}Pb = 36.5646 \pm 0.478\%$; $n = 7$), using the reference values of Catanzaro et al. (1968).

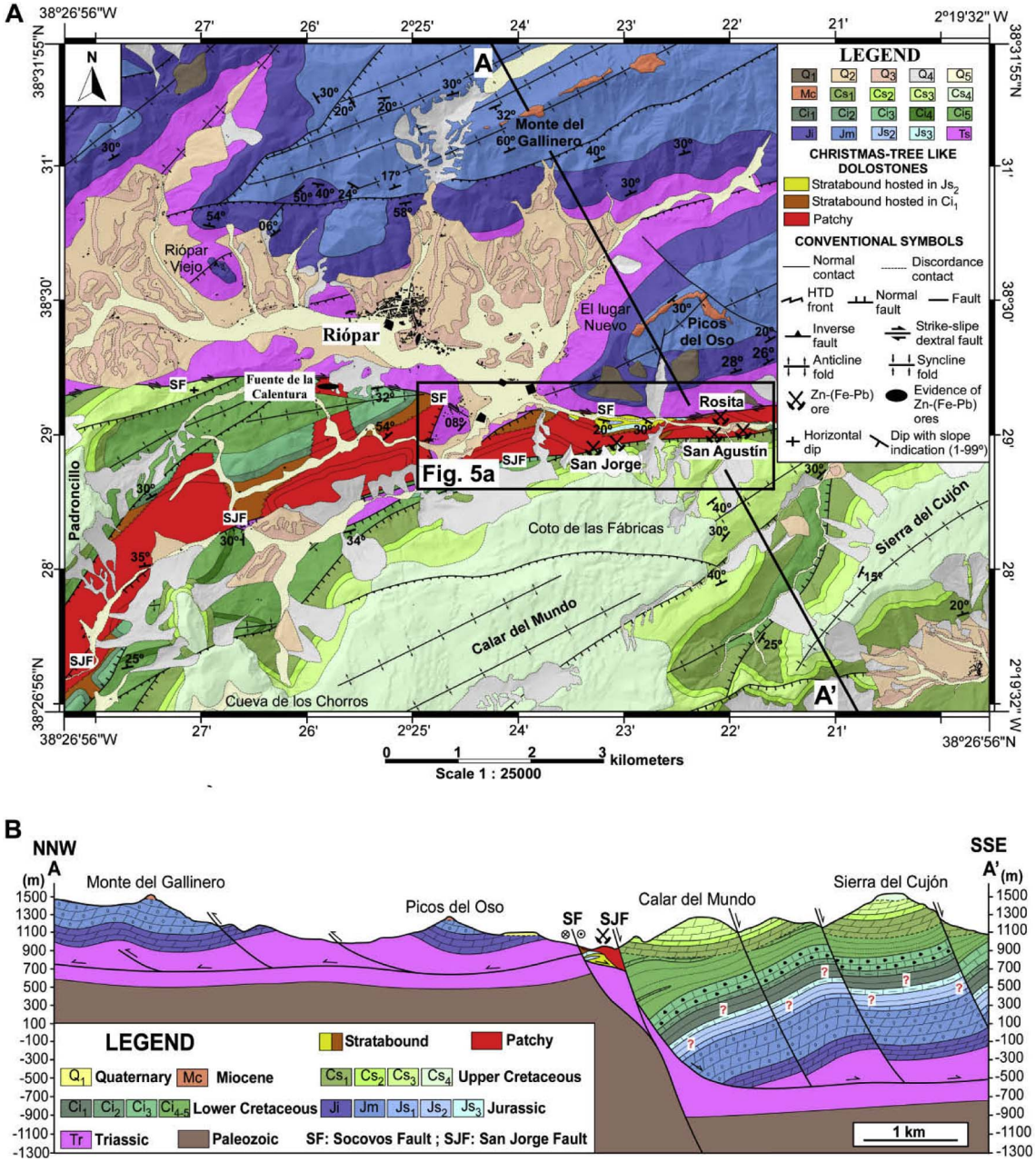

Fig. 3. Geologic map (A) and geologic cross section (B) of the studied area with distribution and morphology of the host dolomite bodies of the Zn-(Fe-Pb) mineralization (see Fig. 4 for detailed geological map). Tr: Triassic clays and sandstones; Ji: Lower Jurassic dolostones; Jm: Middle Jurassic dolostones; Js_1: Upper Oxfordian to Middle Kimmeridgian limestones; Js_2, Js_3, Ci_1: Sierra del Pozo Fm; Ci_2: Cerro Lobo Fm; Ci_3: Arroyo de los Anchos Fm; Ci_4: sandstones and clays of Utrillas facies; Ci_5: dolostones of Utrillas facies; Cs_1, Cs_2, Cs_3: Cenomanian-Turonian dolostones; Cs_4: Coniacian-Santonian limestones; Mc: Miocene polimictic conglomerate; Q_1: undifferentiated colluvium; Q_2: alluvial fans; Q_3: debris on alluvial fans; Q_4: debris on hillsides; Q_5: recent colluvial; SF: Socovos fault; SJF: San Jorge fault.

4. Ore deposits

Mineralization at Riópar consists of a set of small bodies hosted in the Upper Member (Mb) of the Sierra del Pozo dolomitized limestones (Figs. 2 and 3). Pre-ore dolomitization selectively replaced Upper Jurassic to Lower Cretaceous carbonate rocks, forming stratabound bodies and patchy morphologies near San Jorge fault (Figs. 3 and 4). The sulfide Zn-(Fe-Pb) deposits are distributed E to W along a 1.6 km trend. The ore deposit outcrops in the footwall block of the San Jorge fault and is limited to the north by the Socovos strike-slip fault, where the carbonate rocks conform to an anticline fold (Figs. 3 and 4). No sulfide minerals have been recognized in the footwall block of Socovos fault and in the hanging wall block of the San Jorge fault. As the Upper Jurassic and Lower Cretaceous succession does not outcrop in the hanging wall block of the San Jorge fault, the presence of the same dolomitizing and mineralizing process cannot be confirmed (Fig. 3b: red question marks).

The historically mined ore bodies are found in three areas (Fig. 4): San Agustín, with two ore bodies (Sg1, Sg2); Rosita (Ro), in the easternmost part; and San Jorge, in the central part of the studied area, containing several small bodies which are grouped in three occurrences (Sj1, Sj2, Sj3). Considering the accessible mining works and comparing with historical reports (De Botella y Hornos, 1868; De la Escosura, 1845; Pellicio, 1845; Urbano-Vicente, 1972) approximate mean dimensions for San Agustín and San Jorge ore bodies of 20–50 m in high, 50–100 m in length and 20–30 m in width have been inferred (Fig. 5). The mineralization occurs in a variety of forms that include: i) irregular lenses (Fig. 6a) of NW-SE and NE-SW trends, dipping 20–50° to the

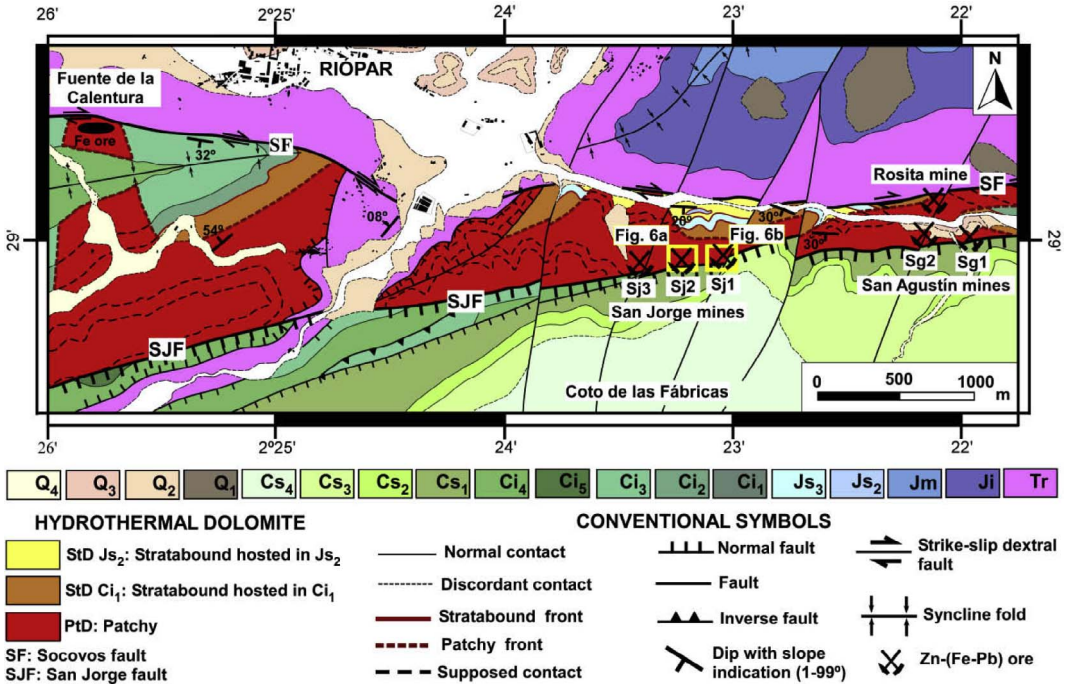

Fig. 4. Detailed geologic map of the Riópar area with the distribution of the hydrothermal dolostone bodies and location of Zn ore deposits (modified from Navarro-Ciurana et al., 2016a). See Fig. 5 for detailed maps of San Jorge mines. Tr: Triassic clays and sandstones; Ji: Lower Jurassic dolostones; Jm: Middle Jurassic dolostones; Js_2, Js_3, Ci_1: Sierra del Pozo Fm; Ci_2: Cerro Lobo Fm; Ci_3: Arroyo de los Anchos Fm; Ci_4: sandstones and clays of Utrillas facies; Ci_5: dolostones of Utrillas facies; Cs_1, Cs_2, Cs_3: Cenomanian-Turonian dolostones; Cs_4: Coniacian-Santonian limestones; Q_1: undifferentiated colluvium; Q_2: alluvial fans; Q_3: debris on alluvial fans; Q_4: recent colluvium.

south, crosscutting the stratification and forming cockade textures (Fig. 6b); ii) small branching bodies parallel to stratification (Fig. 6c) connected to the irregular lenses; iii) ore-cemented breccia zones (Fig. 6a and d); iv) cm- to mm-wide veins and veinlets (Fig. 6e); and v) disseminations and stylolite porosity filling within the host-dolomites (Fig. 6f). Most deposits in this area are characterized by an extensive supergene alteration of the hypogene Zn-Fe-Pb sulfides, resulting in the formation of non-sulfide ("calamine") minerals (Fig. 6c), mainly smithsonite (Navarro-Ciurana et al., 2016c). The discordant lenses associated to branching stratiform ore bodies, the ore-cemented breccias and the veins appear generally near the San Jorge fault rather than the Socovos fault. This contrasts with ore disseminations and host rock replacements, which are the most common occurrences away from the San Jorge fault.

5. Mineralogy, textures and paragenesis

The hypogene mineralogy is quite simple and consists, in order of abundance, of dolomite, marcasite, sphalerite, and galena (Figs. 7 and 8). A detailed petrographic description of several generations of dolomite was presented by Navarro-Ciurana et al., 2016a.

Two types of sphalerite are identified: i) euhedral to subhedral sphalerite (Sph-I), which occurs as disseminations (Fig. 7a) and granular aggregates; and ii) colloform banded sphalerite (Sph-II; Fig. 7b).

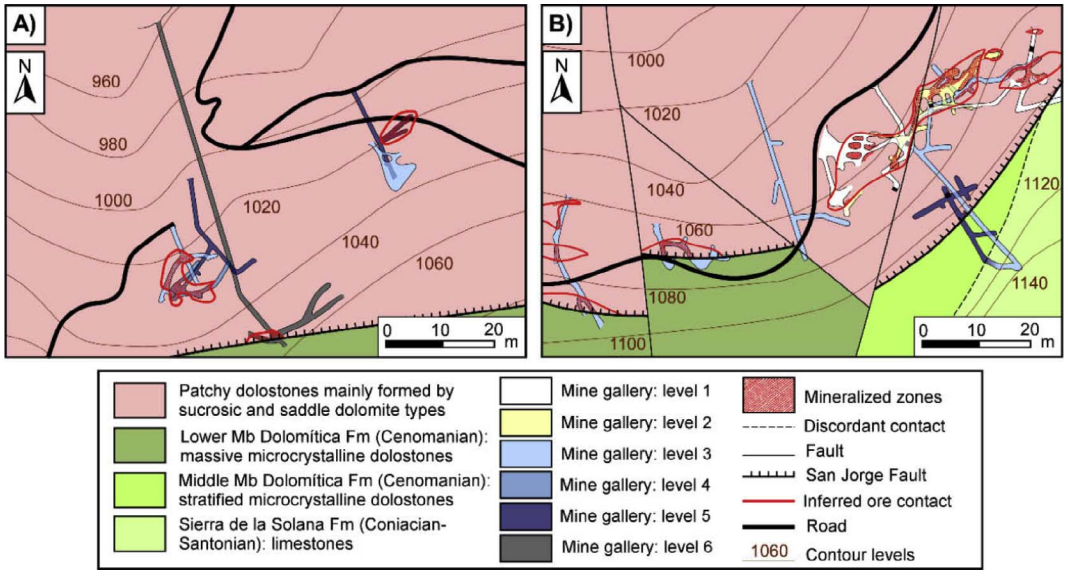

Fig. 5. Detailed maps of San Jorge Sj2 (A) and Sj1 (B) mines with location of exploitation galleries and Zn-(Fe-Pb) mineralized zones (modified from Urbano-Vicente, 1972). See Fig. 4 for mine locations.

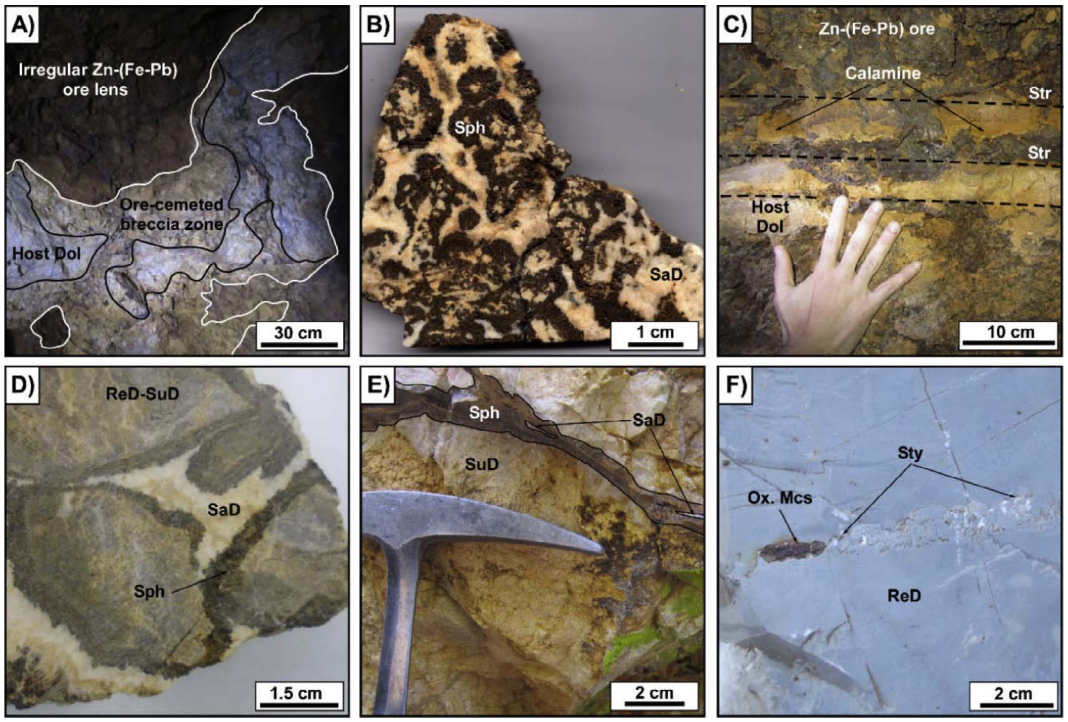

Fig. 6. Mine photographs of Zn-(Fe-Pb) ores. (A) Massive irregular Zn-(Fe-Pb) ore lenses with an ore-cemented breccia zone development. (B) Hand sample of cockade texture mineralization. (C) Stratiform Zn-(Fe-Pb) ore bodies highly altered to Zn-(Fe-Pb) non-sulfide ores ("calamine"). (D) Ore-cemented breccia hand sample. (E) Sphalerite vein associated with saddle dolomite. (F) Oxidized marcasite filling stylolite porosity within host-dolostone (Host Dol: host dolostone; ReD-SuD: replacive to sucrosic dolomite; SuD; sucrosic dolomite; SaD: saddle dolomite; Sph: sphalerite; Ox. Mcs: oxidized marcasite; Str: stratification; Sty: stylolite).

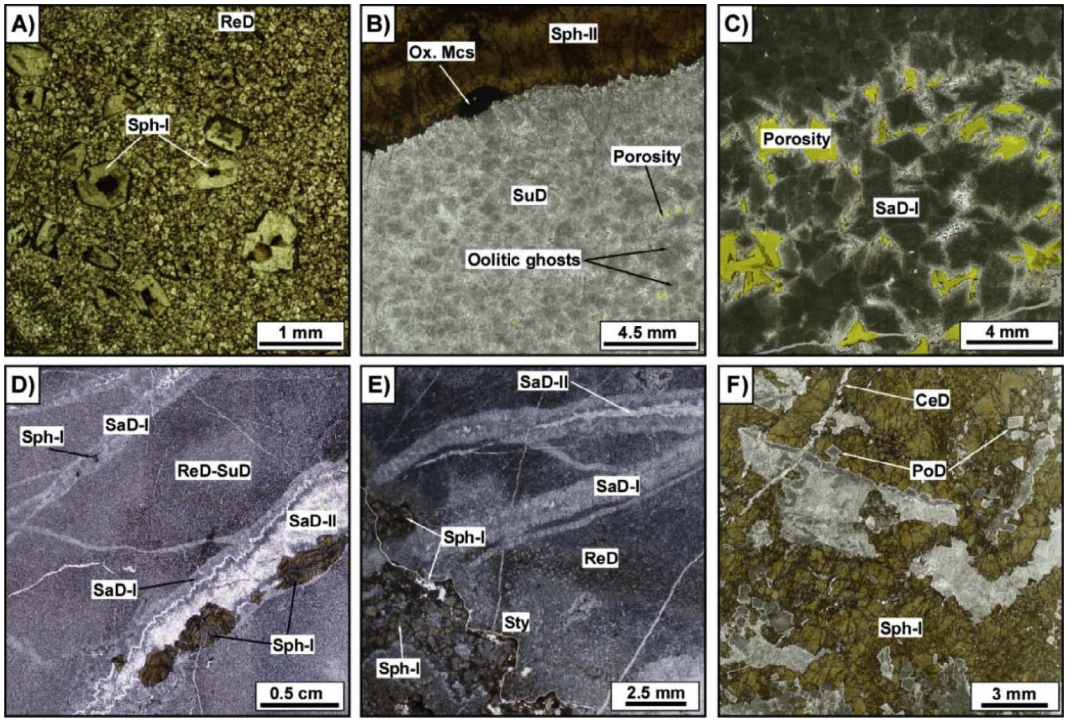

Fig. 7. Transmitted light (TL) photomicrographs. (A) Matrix replacive dolomite (ReD) crystals partially replaced by discrete sphalerite (Sph-I) crystals forming disseminations in the host dolostone. (B) Sucrosic dolomite cements (SuD) with oolitic ghosts and porosity development forming the host dolostone of colloform banded sphalerite (Sph-II) and oxidized marcasite (Ox. Mc) crystals. (C) Grey saddle dolomite cements with dark centers and well-developed intercrystalline porosity (yellow zones). (D) TL photomicrograph showing fracture filling by grey saddle dolomite (SaD-I), sphalerite and milky saddle dolomite (SaD-II) hosted in ReD-SuD transition dolomite. (E) Fractures filled by SaD-I and SaD-II hosted in matrix replacive dolomite (ReD) and discrete sphalerite crystals (Sph-I) replacing ReD phase. Note a stylolite (Sty) that crosscuts the different dolomite types and Sph-I phase. (F) TL photomicrograph showing cockade texture of granular aggregate sphalerite crystals (Sph-I) that extensively replace planar-e porphyrotopic dolomite (PoD) with veins of planar-s cloudy dolomite cement (CeD) crosscutting the previous phases. (For interpretation of the references to color in this figure legend, the reader is referred to the web version of this article.)

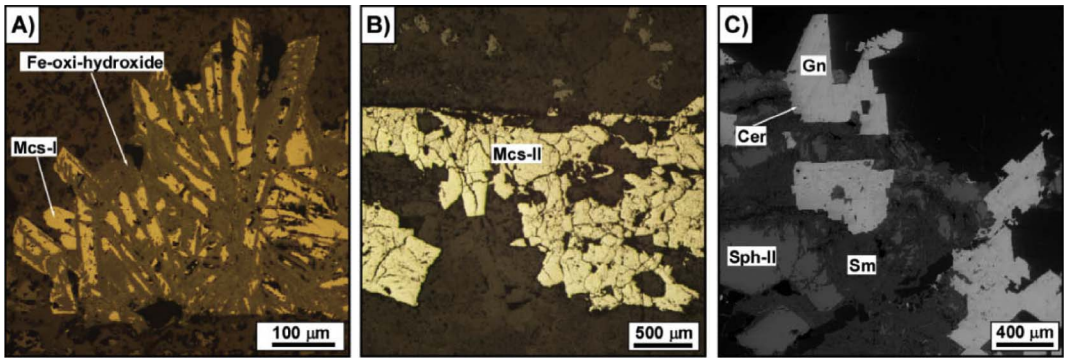

Fig. 8. Petrographic characteristics of marcasite and galena. (A) Reflected light (RL) photomicrograph of radiating cockscomb marcasite crystals (Mcs-I) extensively altered to Fe-oxi-hydroxides. (B) RL image of massive aggregate marcasite (Mcs-II) filling fracture. (C) Cathodoluminescence (CL) image of PoD showing bright red luminescence nucleus. (C) SEM backscattered image of galena (Gn) altered to cerussite (Cer) associated with botryoidal sphalerite (Sph-II) altered to smithsonite (Sm).

Sph-I crystals are roughly equant and range from very fine to coarse in size (100 µm up to 3 mm), with alternating bands of dark to pale brown and red to orange colors (Fig. 7d). Sph-I occurs filling fractures together with saddle dolomite cements (Fig. 7c and d), cementing breccias (Fig. 6d), forming veins (Fig. 7d) and cockade textures (Figs. 6b and 7f). Disseminated sphalerite crystals (> 500 µm) have been observed in the host dolostones and replacing the fine matrix-replacive dolomite crystals of the pre-ore stage (Fig. 7a and e). Colloform sphalerite (Sph-II), which is a less common type than Sph-I, consists of aggregated botryoidal crystals filling mm- to cm-thick fractures (Fig. 7b) and cementing breccias together with saddle dolomite. Furthermore, colloform sphalerite crystals are also zoned, with dark brownish bands and various hues of yellow, orange, and red colors (Fig. 7b).

Marcasite is present in most outcrops, usually extensively altered to Fe-oxi-hydroxides (Fig. 8a and b). Petrographic observations using optical microscopy reveal two marcasite types: radiating cockscomb (Mcs-I) and massive aggregate phases (Mcs-II). Spear-like crystals range from 0.3 mm up to 1 mm in length (Fig. 8a). They are found either filling fractures with sphalerite and saddle dolomite or filling the porosity of stylolites parallel to bedding (Fig. 6f). Massive aggregates of marcasite (Mcs-II) are less common and have been observed in millimeter-size veins associated with sphalerite and saddle dolomite. Marcasite consists of euhedral to subhedral crystals ranging from 30 to 500 µm in size (Fig. 8b).

Galena is the least abundant sulfide mineral and has only been found in a few specimens from the San Jorge dumps. Galena is observed as cubo-octahedral individual and aggregated crystals of 50 µm to 2 mm in size filling fractures with sphalerite, marcasite and saddle dolomite (SaD-II), and replacing host dolostone and partially sphalerite (Fig. 8c).

The mineral paragenetic sequence (Fig. 9) has been established from microscopic textural relationships between dolomite and Zn-Fe-Pb sulfide phases. Previous to precipitation of sulfides, a pre-ore dolomitization stage occurred (Fig. 9), which is characterized by matrix replacive (ReD), euhedral to subhedral sucrosic (SuD) and saddle grey (SaD-I) dolomite crystal types affecting the precursor limestones (Fig. 7). During the hypogene ore stage (Fig. 9), SaD-I dolomite cements also formed filling fractures and breccia porosity previously to Zn-Fe-Pb sulfide (marcasite, sphalerite and galena) precipitation, whereas pinkish to milky saddle dolomite cements (SaD-II) filled remnant porosity after SaD-I and sulfide crystallization (Fig. 7d). Marcasite was the first sulfide phase to precipitate within stylolites (Fig. 6f), porosity and fractures (Fig. 8b) just after SaD-I (Figs. 7b and 9). The paragenetic sequence of the different marcasite types (radiating cockscomb and disseminated and massive aggregates) is unclear due to the absence of textural relationships between them and their extensive alteration to Fe-oxi-hydroxides (Fig. 8a). On the other hand, sphalerite precipitated overgrowing and postdating marcasite (Fig. 7b). The relative chronology of the two sphalerite types has not been determined. Galena was the last sulfide phase to precipitate, filling porosity before SaD-II (Fig. 9) and partially replacing sphalerite, although in some cases, they are observed precipitating cogenetically (Fig. 8c).

During a post-ore dolomitization stage (Fig. 9) sphalerite was extensively replaced by porphyrotopic dolomite (PoD) (Fig. 7f), which caused a decrease in the original abundance of sphalerite. A final dolomitizing fluid pulse must have been responsible for the precipitation of the fine-grained dolomitic cements (CeD) (Fig. 7f).

6. Geochemical data

Results of elemental compositions analyzed with WDS Electron Microprobe (EMP) are presented in Table 1; the redox conditions of precipitations have been inferred from sphalerite compositions (Table 2). S and Pb isotope compositions are summarized in Tables 3 and 4. Only unaltered crystals were chosen for the analyses.

6.1. Sulfide mineral chemistry

Both sphalerite types (Sph-I and -II) were analyzed, revealing a relatively chemical homogeneity (Table 1) in major as well as in trace elements. Zn and S contents fall in the range of 61.26–66.66 wt% and 31.76–33.80 wt% respectively, with averages of 64.81 wt% Zn and 32.94 wt% S for Sph-I (n = 86) and 63.96 wt% Zn and 33.12 wt% S for Sph-II (n = 6). The most important detected minor and trace elements in sphalerite are Fe (0.27–4.73 wt%), Pb (0.09–0.71 wt%), Cd (< 0.51 wt%), Ga (< 0.21 wt%) and Ge (< 0.08 wt%) (Table 1). Other minor and trace element contents detected are Bi (< 0.14 wt%), Sb (< 0.08 wt%), Ag (< 0.06 wt%), Co (< 0.03 wt%), Mn (< 0.02 wt%), In (< 0.03 wt%) and As (< 0.03 wt%).

The Ga/Ge ratios of sphalerite fall between 0.81 and 21.28 (Table 1). These ratios can be used to determine temperatures in the source regions of ore solutions (Kant et al., 2012; Möller, 1985, 1987). This geothemometer is based in the assumption that the elements present in the ore fluid are in equilibrium with rock-forming minerals at the source. As the $(Al/Si)_{total}$ ratio is a function of temperature in hydrothermal systems (e.g., Helgeson, 1969) and the atomic ratio of Ga/Al and Ge/Si is constant in rocks (Möller, 1985), as well as in river water and saline geothermal waters (Arnorsson, 1984) with values very similar to that in the rocks, the $(Ga/Ge)_{total}$ ratio is also expected to be a function of temperature in geothermal fluids (Möller, 1987). The log (Ga/Ge) values vary between −0.09 and 1.59, indicating temperatures from 194 to 252 °C for the fluid source region, with an average of 224 °C (Fig. 10).

Microprobe compositional profiles across two crystals of Sph-I and Sph-II (Fig. 11) reveal different element content from core to rim, particularly in Zn, Fe, Pb and Cd. Although sphalerite is commonly Fe-

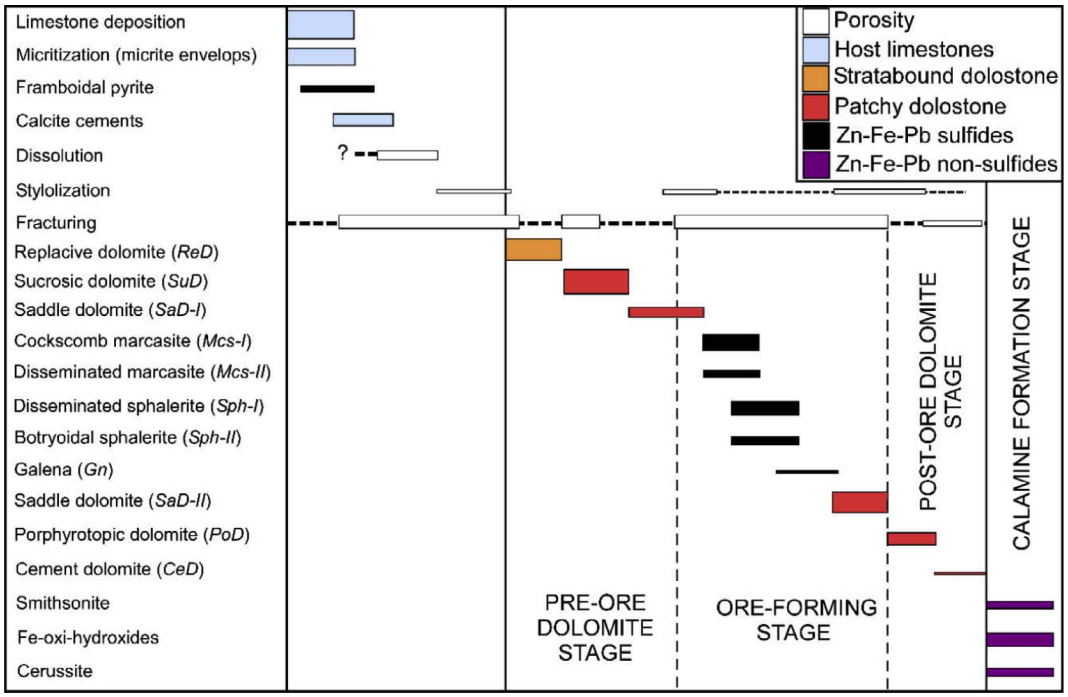

Fig. 9. Summary of the paragenetic succession in the Riópar sulfide Zn-(Fe-Pb) ores with the dolomitization stage according to Navarro-Ciurana et al. (2016a).

poor, the iron content is higher in dark brownish to reddish bands than in pale brownish to yellowish zones (Fig. 11). On the other hand, the X_{FeS} content of sphalerite results in 1.0–23.0 mol% FeS, with an average value of 7.1 ± 5.0 mol% FeS (Table 2), although it displays an asymmetric distribution with the mode at 4.5 mol% FeS (Fig. 12). A correlation between Fe and Zn content is apparent in Sph-I and Sph-II,

Table 1
Electron Microprobe (EMP) analyses of sulfide minerals.

Phase[a]	Zn	S	Fe	Pb	Cd	Ga	Ge	Bi	Sb	Ag	Co	Mn	In	As	Ga/Ge
	(wt.%)														
LOD	0.02	0.01	0.02	0.02	0.01	0.03	0.01	0.01	0.01	0.02	0.01	0.01	0.01	0.02	
Sph-I															
N	86	86	86	86	77	24	16	64	63	14	39	22	23	4	7
Min.	61.26	31.76	0.27	0.09	0.01	0.03	0.01	0.01	0.01	0.02	0.01	0.01	0.01	0.02	0.81
Mean	64.81	32.94	1.44	0.26	0.11	0.09	0.03	0.04	0.05	0.03	0.01	0.01	0.02	0.03	8.26
Max.	66.65	33.80	4.73	0.71	0.51	0.21	0.08	0.14	0.08	0.06	0.03	0.02	0.03	0.03	21.29
St. dv.	1.19	0.47	1.03	0.15	0.11	0.05	0.02	0.03	0.02	0.01	0.01	0.00	0.01	0.01	7.13
Sph-II															
N	6	6	6	6	6	4	1	4	6	–	3	–	2	1	1
Min.	61.62	32.94	0.82	0.16	0.05	0.05	–	0.05	0.01	–	0.01	–	0.01	–	–
Mean	63.96	33.12	1.64	0.43	0.08	0.11	0.01	0.06	0.04	–	0.02	–	0.01	0.02	6.67
Max.	65.15	33.32	2.80	0.63	0.17	0.18	–	0.08	0.07	–	0.03	–	0.02	–	–
St. dv.	1.22	0.15	0.79	0.17	0.04	0.06	–	0.01	0.02	–	0.01	–	0.01	–	–
Mcs-I															
N	1	2	2	2	1	–	1	2	2	–	2	–	1	–	–
Min.	–	53.63	46.08	0.30	–	–	–	0.13	0.03	–	0.08	–	–	–	–
Mean	0.04	53.65	46.20	0.64	0.04	–	0.01	0.16	0.04	–	0.08	–	0.02	–	–
Max.	–	53.68	46.31	0.97	–	–	–	0.19	0.05	–	0.09	–	–	–	–
St. dv.	–	0.04	0.16	0.47	–	–	–	0.04	0.01	–	0.01	–	–	–	–
Mcs-II															
N	–	2	2	2	2	–	–	2	1	–	2	–	–	–	–
Min.	–	52.32	46.34	0.32	0.01	–	–	0.17	–	–	0.10	–	–	–	–
Mean	–	52.39	46.38	0.32	0.01	–	–	0.19	0.04	–	0.10	–	–	–	–
Max.	–	52.46	46.42	0.33	0.01	–	–	0.21	–	–	0.10	–	–	–	–
St. dv.	–	0.10	0.06	0.00	0.00	–	–	0.02	–	–	0.00	–	–	–	–
Gn															
N	–	7	4	7	7	3	4	7	7	–	2	–	1	–	–
Min.	–	13.11	0.02	85.47	0.06	0.04	0.01	0.11	0.04	–	0.01	–	–	–	–
Mean	–	13.31	0.02	85.98	0.12	0.06	0.03	0.20	0.07	–	0.02	–	0.01	–	–
Max.	–	13.54	0.03	86.26	0.16	0.09	0.04	0.27	0.16	–	0.03	–	–	–	–
St. dv.	–	0.14	0.01	0.27	0.04	0.02	0.01	0.06	0.04	–	0.01	–	–	–	–

[a] *LOD*: Limit of detection of the Electron Microprobe for each element; *Sph-I*: disseminated and granular aggregate sphalerite; *Sph-II*: colloform banded sphalerite; *Mcs-I*: radiating cockscomb marcasite; *Mcs-II*: disseminated and massive aggregate marcasite; *Gn*: galena; *n*: number of analyses; Min. minimum value; Mean: mean value; Max.: maximum value; St. dv.: standard deviation.

Table 2
log fO_2 calculated from FeS content in sphalerite at 200 °C.

Phase[a]	FeS	Log fO_2		
	% molar	(log $\alpha H_2S = -1$)	(log $\alpha H_2S = -3$)	(log $\alpha H_2S = -5$)
Sph				
N	92	92	92	92
Min.	22.97	−49.40	−45.40	−41.40
Mean	7.05	−48.25	−44.25	−40.25
Max.	0.98	−46.77	−42.77	−38.77
St. dv.	4.99	0.60	0.60	0.60

[a] *Sph*: sphalerite; *n*: number of analyses; Min. minimum value; Mean: mean value; Max.: maximum value; St. dv.: standard deviation.

Table 3
Sulfur isotope compositions of sulfide minerals from the Riópar Zn-(Fe-Pb) ore deposit.

Spot No.	Sample No.	Phase type	$\delta^{34}S$ (CDT)	σ ($\delta^{34}S$)
1	JO-20a-1	Galena	−2.56	0.09
2	JO-20b-1	Galena	−2.41	0.09
3	JO-20a-3	Galena	−2.8	0.1
4	SG-02b-1	Marcasite	−7.51	0.09
5	SJ-41a-2	Marcasite	−6.95	0.09
6	SJ-42a-1	Marcasite	−5.84	0.09
7	SJ-42a-2	Marcasite	−6.04	0.09
8	JO-20d	Sphalerite	−1.64	0.09
9	SG-02a-1	Sphalerite	−2.25	0.09
10	SG-02a-2	Sphalerite	−1.88	0.09
11	SG-05c	Sphalerite	0.66	0.09
12	SG-07	Sphalerite	3.48	0.09
13	SJ-41a-1	Sphalerite	1.47	0.09
14	SJ-41b	Sphalerite	1.47	0.09
15	RO-03-1	Sphalerite	1.56	0.09
16	RO-17	Sphalerite	0.79	0.09
17	JO-20b-2	Sphalerite	1.5	0.1

which is caused by the substitution of Zn by Fe. Moreover, a high negative correlation ($R^2 = 0.85$) is found between Zn and (Fe + Pb + Cd), indicating that Pb and Cd also substitute for Zn ions (Fig. 13). The Cd content in Sph-I is higher in dark bands than in pale color zones, whereas in Sph-II, Cd shows a progressive enrichment from core to rim but unrelated to color bands (Fig. 11). An inverse correlation between Cd and Pb is observed in Sph-II but not in Sph-I (Fig. 11), which suggests that these two elements may behave antithetically.

Both marcasite phases also appear to be chemically homogeneous (Table 1). They contain 46.08–46.42 wt% Fe and 52.32–53.68 wt% S ($n = 4$), with average of 46.20 wt% Fe and 53.65 wt% S for Mcs-I and 46.38 wt% Fe and 52.39 wt% S for Mcs-II. Pb and Bi have been detected as minor elements, with contents of 0.30 to 0.97 wt% Pb and 0.13 to 0.21 wt% Bi. Other minor and trace element contents detected are Co (< 0.1 wt%), Sb (< 0.05 wt%), Zn, Cd and In (Table 1). Moreover, a high negative correlation ($R^2 = 0.9$) is found between Fe and Pb + Cd + Zn, pointing to a Fe substitution by these metals (Fig. 13).

Results of cubo-octahedral galena microprobe analyses are also listed in Table 1. Lead concentration in galena varies from 85.47 to 86.26 wt%, with an average of 85.98 wt% ($n = 7$). S content is in the range of 13.11–13.54 wt%, with a mean value of 13.31 wt% ($n = 4$). The most important detected minor and trace elements in galena are Bi

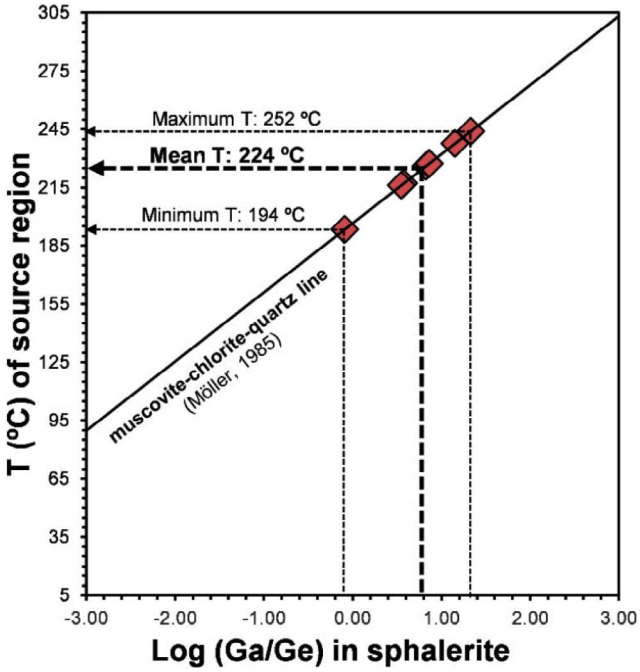

Fig. 10. Plot showing the dependence between log(Ga/Ge) ratios in sphalerite and ore solution temperature in the source region. This graph is based on existing Al/Si geothermometers. The muscovite-chlorite-quartz line is the chlorite geothermometer in the Al/Si system (Möller, 1985, 1987).

(0.11–0.27 wt%), Cd (0.06–0.16 wt%), Sb (0.04–0.16 wt%), Ga (0.04–0.09 wt%), Ge (0.01–0.04 wt%), Fe (0.02–0.03 wt%) and Co (0.01–0.03 wt%) (Table 1).

6.2. Sulfur and lead isotopes

$\delta^{34}S$ values of sphalerite, marcasite, galena and gypsum were reported by Navarro-Ciurana et al. (2016c) to estimate the sulfur source in supergene sulfates related to the oxidation of hypogene sulfide minerals. Here, we discuss the origin of sulfur in sulfide minerals and the temperature of ore formation.

Sulfur isotope composition of sulfide and sulfate minerals is shown in Table 3 and Fig. 14. $\delta^{34}S$ of marcasite ranges from −7.5 to −5.8‰ (average of −6.6‰; $n = 4$), and is isotopically lighter than sphalerite and galena, which have values from −2.2 to +3.5‰ (mean at +0.5‰; $n = 10$) and −2.8 to −2.4‰ (average of −2.6‰; $n = 3$), respectively. Comparing the different mineralizations, no significant $\delta^{34}S$ variations have been observed, suggesting a single sulfur source at the district scale. Systematically, $\delta^{34}S$ values of galena are lower than sphalerite, which, together with the absence of replacement textures, suggest that both sulfides might have precipitated in isotopic equilibrium, and therefore, they have been used as isotope geothermometer (Ohmoto and Rye, 1979). In a sample where both sulfides coexisted, $\Delta^{34}S_{sph\text{-}gn} = 3.9‰$ equivalent to an equilibrium temperature of 159 ± 15 °C (calculated from the equation of Ohmoto and Rye, 1979). This temperature falls within the range of minimum precipitation temperatures obtained from fluid inclusions in sphalerite and gangue dolomite

Table 4
Lead isotope compositions of sulfide minerals from the Riópar Zn-(Fe-Pb) ore deposit.

Spot No.	Sample No.	Phase type	$^{206}Pb/^{204}Pb$ (2σ)	$^{207}Pb/^{204}Pb$ (2σ)	$^{207}Pb/^{204}Pb$ (2σ)
1	JO-20a-1	Galena	18.736 ± 0.002	15.629 ± 0.002	38.496 ± 0.007
2	JO-20a-2	Galena	18.762 ± 0.001	15.660 ± 0.001	38.595 ± 0.002
3	JO-20d-1	Galena	18.748 ± 0.001	15.643 ± 0.001	38.536 ± 0.001
4	JO-20d-2	Galena	18.750 ± 0.001	15.644 ± 0.001	38.548 ± 0.004

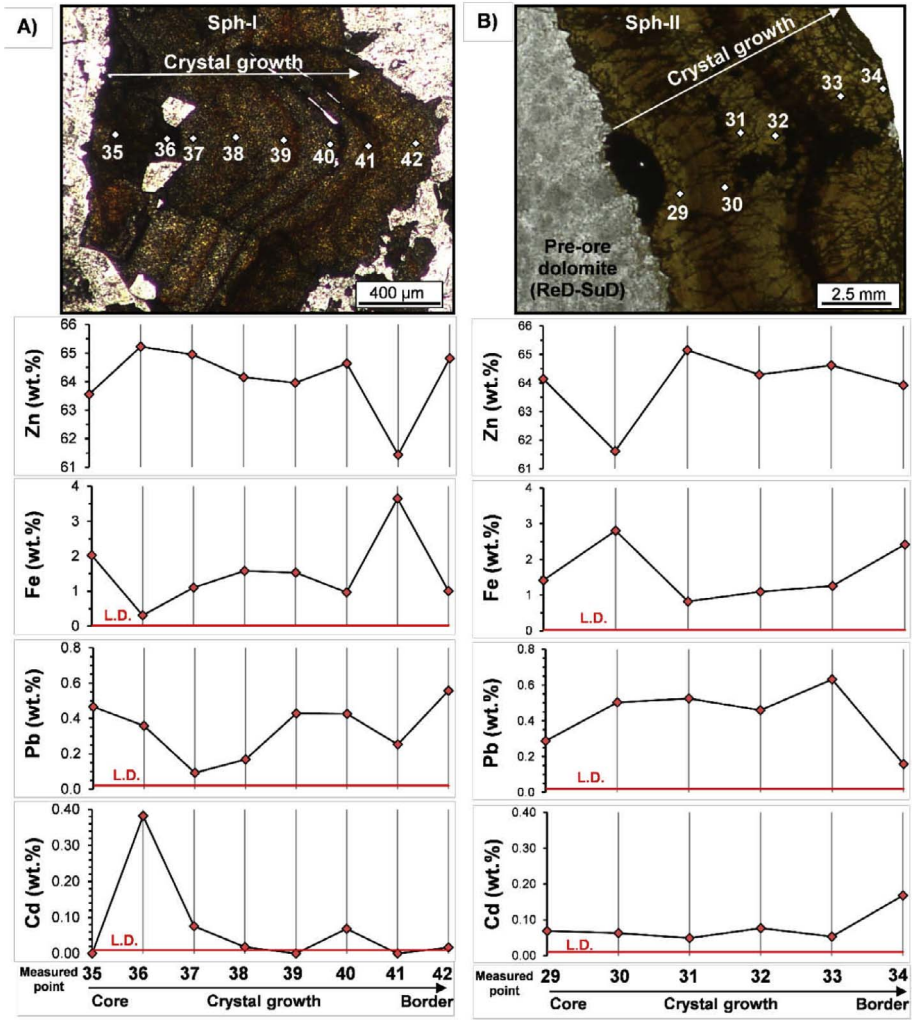

Fig. 11. Wavelength Dispersion Spectrometry (WDS) microprobe profile analyses (Zn, Fe, Pb Cd) performed along disseminated and granular aggregates (Sph-I) as well as colloform banded (Sph-II) sphalerite crystals from center to border (L.D.: limit of detection).

(150–250 °C; Navarro-Ciurana et al., 2016a).

The lead isotope compositions of galena are homogeneous (Table 4 and Fig. 15). $^{206}Pb/^{204}Pb$ ratios range from 18.736 to 18.762, with an average at 18.749. $^{207}Pb/^{204}Pb$ ratios are comprised between 15.629 and 15.660, with a mean value of 15.644; and the $^{208}Pb/^{204}Pb$ ratio ranges from 38.496 to 38.595 with an average of 38.544.

7. Discussion

The presence of replacement and open-space filling textures of sulfides, fault-related stratabound patchy dolomites associated with the sulfide mineralization, and the discordant bedding ore bodies (Figs. 4, 6 and 7) are clear evidences of an epigenetic origin of mineralizations and allow the studied deposits as Mississippi Valley-type (MVT) (e.g., Leach and Sangster, 1993). Colloform and fine grained textures are the result of fast growth precipitation under high supersaturation conditions whereas large and idiomorphic crystals suggest slow growth at low degrees of saturation (e.g., Anderson, 2008). As both types of textures coexist at Riópar, spatial distribution or temporal changes of saturation degree or/and different mechanism of sulfide precipitation probably occurred in the studied area. Mineralogy, textures and chemical composition are similar to other MVT deposits of the Iberian Peninsula (e.g., Reocín mine, Basque-Cantabrian Basin, N Spain: Velasco et al., 2003; Mas de la Mina-Cedramán and Valdelinares deposits, Maestrat Basin, E Spain: Grandia et al., 2003a).

Furthermore, fault-related Zn-Pb occurrences within Lower Cretaceous dolomitized carbonates are a common feature of the Prebetic Zone (Upper Hauterivian-Valanginian), Maestrat (Aptian) and Basque-Cantabrian (Aptian-Albian) MVT ore districts, suggesting similar stratigraphic and/or tectonic controls in the formation of these deposits. In the Riópar area, mineralization is spatially related to the San Jorge fault (Fig. 4), indicating that this fault likely as a major conduit for a metal-bearing fluid flowing from the source region to the precipitation site. The temperature from sphalerite Ga/Ge geothermometer (194–252 °C; average ~225 °C) and the sulfur isotope equilibrium temperature (159 ± 15 °C) are different, but overlap with the T_h range obtained in fluid inclusions from ore-stage dolomite and sphalerite (150–250 °C; Navarro-Ciurana et al., 2016a), indicating that the temperature of the hydrothermal metal-bearing fluid did not vary substantially between the reservoir and the precipitation area. This fact suggests a closeness between both sites and/or a rapid upflow along the San Jorge fault. Assuming a temperature of 225 °C and a geothermal gradient of 33 °C/km, the hydrothermal reservoir region could be located at a depth of around 6–7 km.

The wide range in the Fe content of sphalerite (0.27–14.38 wt%; Table 1) may be caused by a binary fluid mixing if (1) the Fe content in both fluids is different and/or (2) by changes in the oxygen fugacity conditions during precipitation of this mineral (e.g., Barton and Toulmin, 1966; Czamanske, 1974; Scott, 1983). fO_2 conditions during sphalerite precipitation can be estimated from the X_{FeS} content (1.0–23.0 mol% FeS; Table 2 and Fig. 12a) assuming equilibrium with pyrite. The amount of FeS in solid solution in sphalerite (X_{FeS}) is a function of temperature, pressure, and FeS activity (αFeS). According to Scott (1974), αFeS can be calculated as follows:

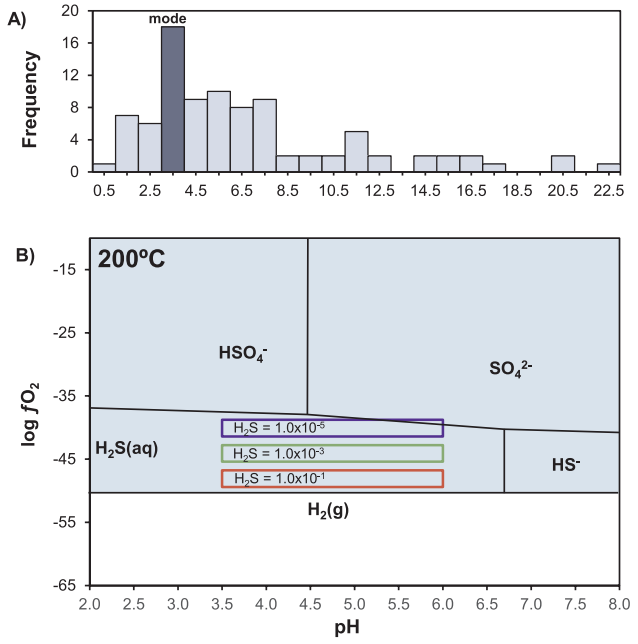

Fig. 12. (A) Histogram of FeS mol% for 92 analyzed sphalerites. (B) log fO_2 vs pH diagram showing the stability field for sulfur species at 200 °C (conditions: P = 100 bars; logαSO_4^{2-} = −6; αH_2O = −6). A pH range from 3.5 to 6 was assumed, which is a typical range of metalliferous basinal brines (Cooke et al., 2000). Calculations of log fO_2 are based on the FeS content in sphalerite according to the equation of Scott (1974) at different H_2S activities of 1.0×10^{-1}, 1.0×10^{-3} and 1.0×10^{-5}.

$\alpha FeS = 0.0257(\text{mol\% FeS}) - 0.00014\ (\text{mol\% FeS})^2$.

Taking a temperature of 200 °C for ore formation (Navarro-Ciurana et al., 2016a) and assuming H_2S concentrations of 1.0×10^{-1}, 1.0×10^{-3} and 1.0×10^{-5} m, the calculated log fO_2 ranges between −49.40 and −46.77 atm, −45.40 and −42.77 atm, and −41.40 and −38.77 atm respectively (Table 2). In a pH-log fO_2 plot (Fig. 12b), and assuming a pH range of 3.5 to 6, a typical range of metalliferous brines (Cooke et al., 2000) compatible with the acidic conditions for the presence of marcasite (Murowchick and Barnes, 1986; Plumlee et al., 1994), log fO_2 values fall within the H_2S stability field. On the other hand, a less acidic pH of the dolomitizing and ore-bearing fluids due to buffering by the interaction with carbonate host rocks cannot be discarded (Navarro-Ciurana et al., 2016a). In any case, assuming a pH close to neutral, the calculated fO_2 values also fall within the H_2S stability field.

7.1. Source of sulfur

The lognormal or gaussian distribution of $\delta^{34}S$ values, with a mode between +1 and +2‰ and a median value of +0.52‰ (Table 3 and Fig. 14), suggests a single sulfur source during the ore formation. The range of $\delta^{34}S$ values (Table 3 and Fig. 14a) of each sulfide mineral (marcasite: −7.5 to −5.8‰; galena: −2.8 to −2.4‰ and sphalerite: −2.8 to +3.5‰), may be explained by slight changes of oxygen fugacity and/or temperature of the hydrothermal fluid during the precipitation of sulfides.

The most common sulfur source in MVT environments is organically bound sulfur, H_2S reservoir gas derived from the reduction of sulfate evaporites, seawater, connate water, or basinal brines. Therefore, a reduction mechanism of sulfate to sulfide is needed: either bacteriologically (BSR) or thermochemically (TSR) mediated. The reduced sulfur involved in sulfide precipitation was most likely produced by TSR as supported by the high precipitation temperatures (150–250 °C; Navarro-Ciurana et al., 2016a).

The most probable sulfur source at Riópar is evaporitic sulfate.

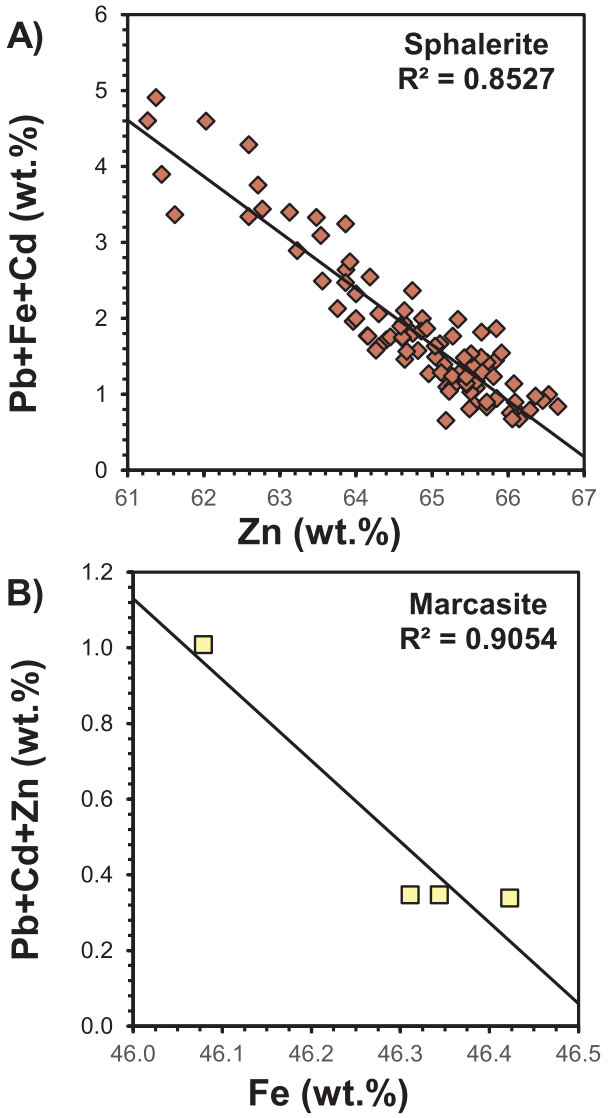

Fig. 13. Binary plots of various metal concentration in sulfide minerals. (A) Zn vs. Pb + Fe + Cd contents in sphalerite; (B) Fe vs. Pb + Cd + Zn content in marcasite.

Gypsum is widespread in the Internal and External Zones of the Betic Cordillera (including the Riópar area) within sediments of Upper Triassic age (Keuper Fm). The $\delta^{34}S$ of this gypsum ranges from +12.5 to +16.6‰ (Ortí et al., 2014), consistent with the values reported by Claypool et al. (1980) and Paytan et al. (2004) for seawater sulfate during Triassic times. The lowest $\delta^{34}S$ value of the Riópar sulfides (marcasite: −7.5‰; Table 3) is 20–24‰ lower than the range values for Triassic evaporites, whereas the highest (+3.5‰; Table 3) is 9–13‰ lighter (Fig. 14b). These sulfate-sulfide isotope fractionations are consistent with the kinetic effect associated with TSR, which produces H_2S 10–20‰ lighter than the precursor sulfate (Machel et al., 1995). Thermochemical reduction of younger marine sulfate of Jurassic to Cenozoic times, with $\delta^{34}S \approx +20$ to +25‰, would produce H_2S isotopically heavier. Therefore, the sulfur source involved during the formation of sulfides would be compatible with a thermochemical reduction of sulfate (dissolved evaporites and/or seawater) of Triassic age (Fig. 14b). Furthermore, Sr-isotope data from gangue dolomites related to sulfide minerals (Navarro-Ciurana et al., 2016a) show a radiogenic signature more compatible with interaction of fluids and siliciclastic rocks, especially abundant among the Triassic sediments, than with Jurassic or Cretaceous marine carbonates.

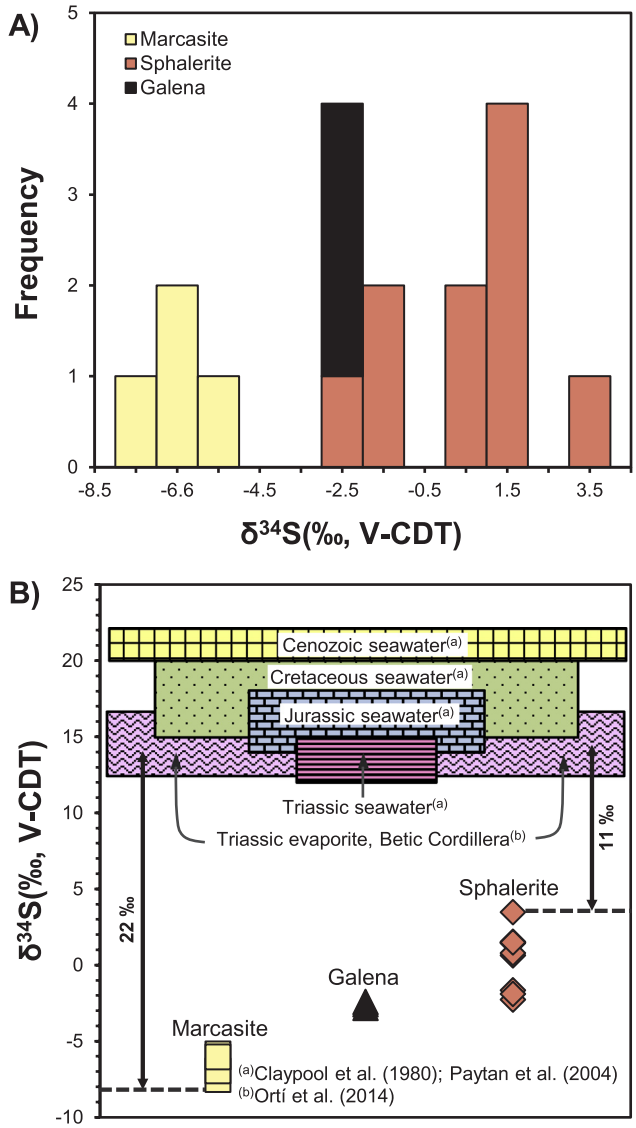

Fig. 14. (A) Histogram of the sulfur isotope compositions of sulfide minerals from the Riópar Zn-(Fe-Pb) ore deposit. (B) Comparison of $\delta^{34}S$ values of sulfide minerals with Cenozoic, Cretaceous, Jurassic and Triassic seawater sulfur isotope composition (Claypool et al., 1980; Paytan et al., 2004), as well as with the Triassic evaporites of the Betic Cordillera (Ortí et al., 2014).

7.2. Source of metals

Pb isotope values from galenas (Table 4) are homogeneous. In the $^{208}Pb/^{204}Pb$-$^{206}Pb/^{204}Pb$ and $^{207}Pb/^{204}Pb$-$^{206}Pb/^{204}Pb$ plots, data are within the analytical uncertainty (2σ). Based on the "plumbotectonics" model of Zartman and Doe (1981) for the growth curves of isotopic Pb, the $^{208}Pb/^{204}Pb$-$^{206}Pb/^{204}Pb$ and the $^{207}Pb/^{204}Pb$-$^{206}Pb/^{204}Pb$ ratios plot in the field below the upper crustal evolution curve and above the orogenic growth curve (Fig. 15), indicating that Pb was predominantly derived from continental crustal rocks. Furthermore, these values plot within the lead isotope field of other Zn-Pb deposits hosted in Lower Cretaceous rocks of the Iberian Peninsula (Fig. 15), including stratabound, SEDEX and vein deposits from the Basque-Cantabrian (Velasco et al., 1996) and Maestrat (Grandia, 2000) basins. Nevertheless, galenas from Riópar are more radiogenic than those from Sierra de Gádor and Sierra Alhamilla stratabound F-Pb-Zn-(Ba) MVT deposits (Internal Zones of the Betic Cordillera, SE Spain) (Arribas and Tosdal, 1994; Fig. 15), which are hosted by carbonates of Triassic age.

Given the homogeneous Pb-isotope composition of galena, the

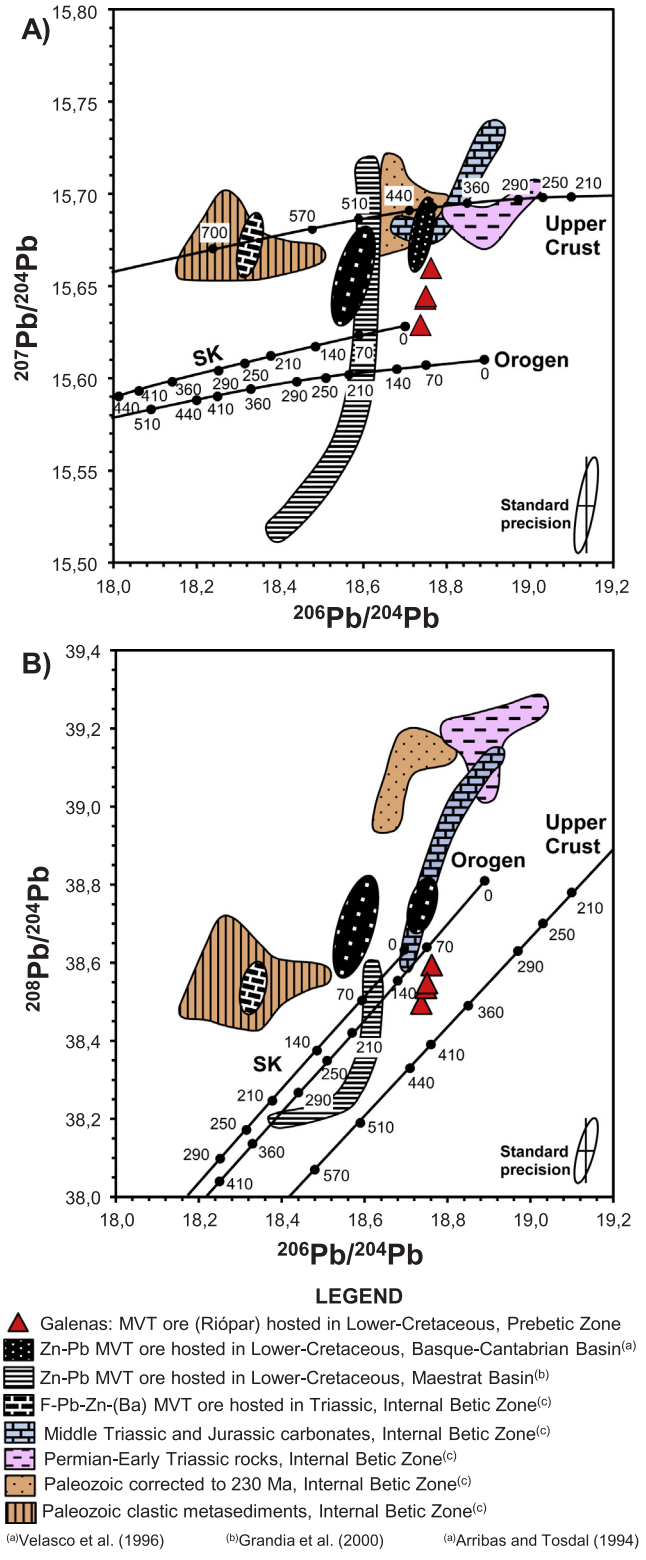

Fig. 15. $^{206}Pb/^{204}Pb$ vs. $^{207}Pb/^{204}Pb$ (A) and $^{206}Pb/^{204}Pb$ vs. $^{208}Pb/^{204}Pb$ (B) diagrams of the Riópar galenas hosted in Lower Cretaceous rocks of the Prebetic Zone. Obtained data is compared with values of other MVT ore deposits in the Iberian Peninsula (data from: Arribas and Tosdal, 1994; Velasco et al., 1996; Grandia et al., 2000). Lead isotopic evolution curves for the upper crust and orogen are according to the plumbotectonic models of Zartman and Doe (1981). SK is the Stacey and Kramers (1975) average crustal Pb growth curve. Isotopic compositions are present-day values and are not corrected for age, except for Paleozoic clastic metasedimentary rocks of the Internal Betic Zone, in which Pb values are corrected to 230 Ma.

origin of lead at Riópar can be related either to a single source or alternatively, to isotopically heterogeneous sources that mixed and homogenized before galena precipitation. In the $^{207}Pb/^{204}Pb$-$^{206}Pb/^{204}Pb$ diagram, galenas plot close to the fields of Paleozoic, Permian-Middle Triassic sediments and Jurassic carbonates. However, in the thorogenic plot ($^{208}Pb/^{204}Pb$-$^{206}Pb/^{204}Pb$) galenas plot well below these fields indicating that source rocks had a low Th/U ratio. Compared to the analyzed galenas, the lead isotope composition of Triassic rocks (Fig. 15: Arribas and Tosdal, 1994) show a distinctly more radiogenic signature, excluding these rocks as the lead source of the sulfide mineralization. Additionally, Jurassic rocks are mainly carbonates and therefore they are not probably the principal source of lead. Hence, Paleozoic basement rocks are the most plausible metal source. This is consistent with the spatial relationship between the deposits and the San Jorge fault, which is probably a reactivation of an old Variscan fault that cross cut the Paleozoic basement and allowed the migration of hydrothermal fluid. Moreover, this hypothesis is consistent with lead isotope compositions from other MVT deposits (Leach et al., 2005) that suggest a relationship between the Pb isotopic composition in a district and the composition of the corresponding basement rocks (Muchez et al., 2005). The difference in the $^{207}Pb/^{204}Pb$ and $^{208}Pb/^{204}Pb$ ratios between Paleozoic metasedimentary rocks of the Internal Betic Zones and the Riópar galena points to an inhomogeneous Paleozoic basement, with lower $^{238}U/^{204}Pb$ and $^{232}Th/^{204}Pb$ ratios in the External parts.

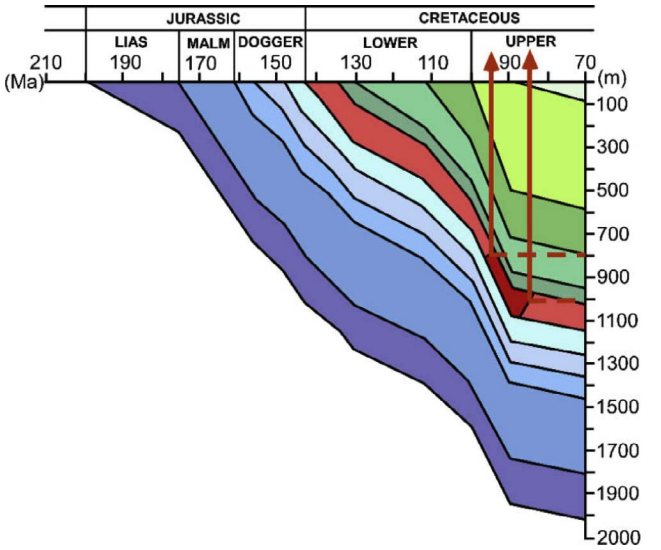

Fig. 16. Jurassic to Cretaceous decompacted subsidence curves showing the most probable time and burial depth (dark red area; 300–500 m) for the formation of stylolitization, hydrothermal dolostone, and MVT mineralization in the Riópar area (orange line). The dashed red line denotes the inferred maximum burial depth at which stylolitization took place. (For interpretation of the references to color in this figure legend, the reader is referred to the web version of this article.)

7.3. Timing

Field relationships and sediment burial depths required for stylolite development can be used to constrain the relative timing (minimum and maximum age) of the ore formation, as no absolute age of the mineralization is available. As mineralization and associated dolomitization occur after lithification (epigenetic origin) of the Upper Mb of the Sierra del Pozo carbonates (Upper Berriasian to Lower Valanginian: Fig. 2), a younger age than 140 Ma for dolomitization and mineralization is suggested. Field evidence suggests that mineralization was affected by minor N-S fault systems generated by the formation of the Betic Chain in relation to the Alpine orogeny (Navarro-Ciurana et al., 2016c; Fig. 4), constraining the ores to be not younger than Miocene (~20 Ma). This is consistent with the results of paleomagnetic dating performed on the Reocín deposit, which indicate a maximum age of 25 Ma (15 ± 10 Ma; Symons et al., 2009).

The host hydrothermal dolomites are characterized by stylolites parallel to bedding filled with sulfides (Fig. 6f). In limestones, stylolites parallel to bedding are commonly formed at depths greater than 800 m (e.g., Dunnington, 1967; Lind, 1993; Nicolaides and Wallace, 1997). However, as dolostones display higher resistance to dissolution, stylolites in these rocks require greater depths (e.g., Mountjoy and Amthor, 1994). In any case, if we assume the depth range reached by the carbonates of Upper Jurassic to Lower Cretaceous ages at Riópar of 800–1000 m, bedding parallel stylolization may have occurred during Upper Cretaceous (95–85 Ma; Fig. 16). As mineralization post-dates stylolite development and pre-dates Alpine tectonic structures (e.g., N-S faults) a period of 95–85 to 20 Ma (Upper Cretaceous-Tertiary) can be inferred for the Zn-(Fe-Pb) ore formation. This range is in agreement with the ages of hydrothermal fluid migration leading to Hg-Sb mineralization and Zn-Pb ore deposits in the Maestrat Basin, that occurred during Santonian (85 ± 3 Ma; Tritlla and Solé, 1999) and Early Paleocene (62.6 ± 0.7 Ma; Grandia et al., 2000) respectively.

Navarro-Ciurana et al., 2016a demonstrated the relationship between dolomitizing and ore-bearing fluids in the Riópar area. The similarity in major element compositions and C/O isotopic values ($\delta^{13}C$: −2.3 to +0.9‰; $\delta^{18}O$: +25.1 to 27.6‰) for host dolostones and gangue dolomites related to sulfide minerals, suggests uniform chemical conditions during dolomitization and mineralization, supporting the idea of a continuous hydrothermal dolomitizing and mineralizing process. Furthermore, this idea is supported by the overlapping homogenization temperatures in fluid inclusions from host rock dolomites, sphalerite and related gangue dolomites (Navarro-Ciurana et al., 2016a). Therefore, a restricted period of time for the formation of host dolostone and mineralization, which must allow uniform chemical and physical conditions of the hydrothermal system, is required. As the hydrothermal host dolostones and mineralization pre- and post-date stylolites respectively, and the formation of the Riópar dolomitization and mineralization is related with the same hydrothermal processes in a restricted period of time, an Upper Cretaceous age, as in the Maestrat basin, is suggested for the dolomitization, stylolitization and mineralization processes.

7.4. Ore controls

Dolomitization and associated MVT mineralization at Riópar resulted from different causes. Stratigraphy may be one of them, as pre-ore stratabound matrix replacive dolomites only affect the Lower and Upper Mb of Sierra del Pozo Fm (Late Jurassic-Early Cretaceous). This fact suggests physical (e.g. permeability, size of particles) and chemical characteristics (e.g. mineralogy) of the precursor limestone controlled mineralization, as previously discussed by Navarro-Ciurana et al., 2016a.

The Upper Mb of the Sierra del Pozo carbonate formation (Fig. 2) exerted a strong control on the emplacement of the deposits, as the economic Zn occurrences are spatially and temporally associated with saddle dolomite. The enhanced porosity and permeability associated with the regional pre-ore dolomitization (Fig. 7c) appear to have been a critical factor in determining the size and the geometry of the Riópar ore bodies (Navarro-Ciurana et al. 2016a). The variety of ore morphologies recognized in an ore body (disseminations, stylolites, discordant lenses, branching offshoots, ore-cemented breccias and fractures) indicates there was also a tectonic control (e.g., faults, fractures and brecciation). A larger scale structural control is also deduced from the presence of patchy dolostones and Zn occurrences closer to San Jorge fault. Therefore, the contribution of the dolomitization and mineralization fluid from the Socovos fault must have been low to moderate, in contrast with the influx of hydrothermal fluids from the San Jorge fault, indicating a structurally-controlled fluid circulation.

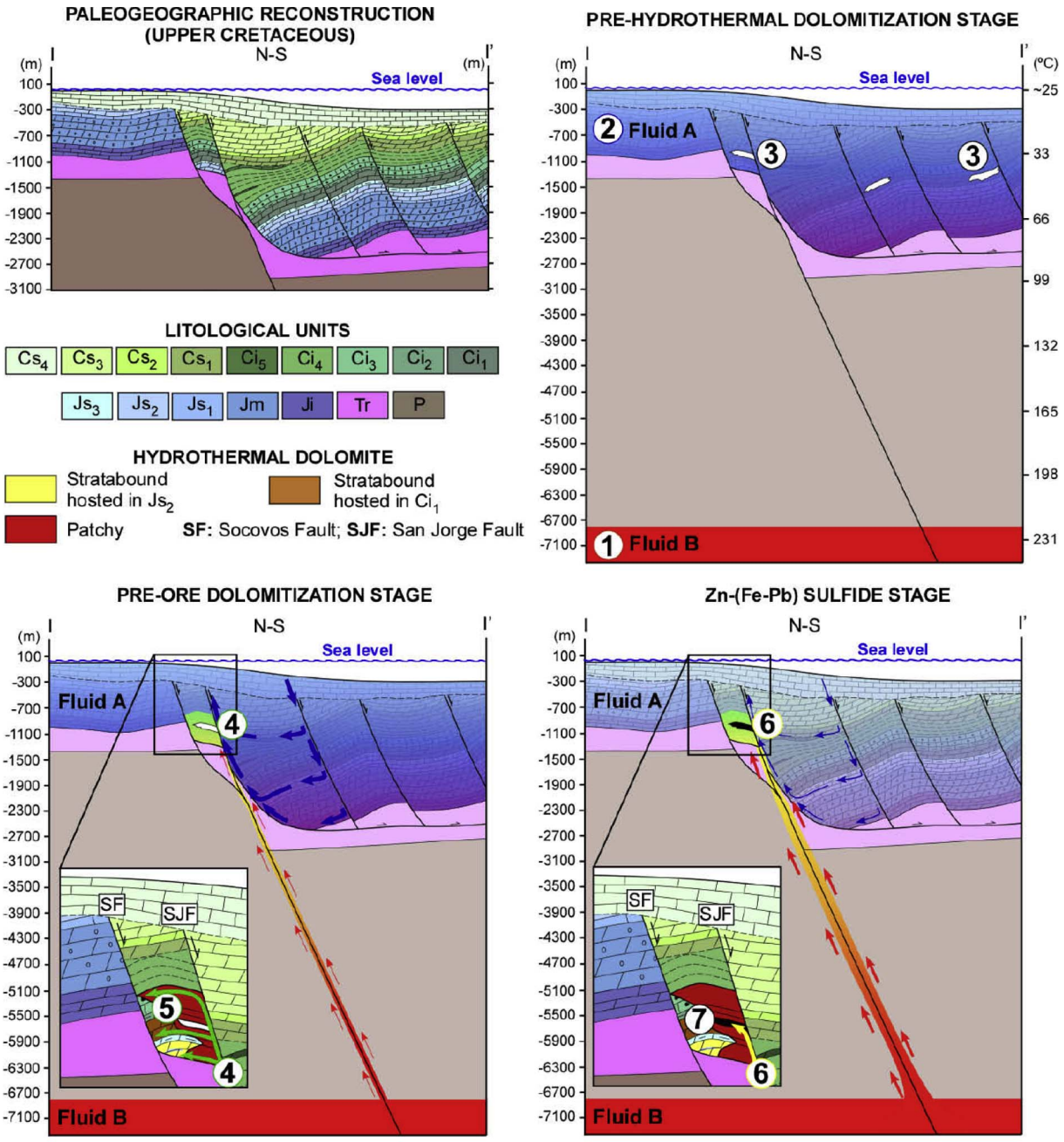

(1) Fluid B: Hydrothermal (~225 ºC) high-salinity (> 25 wt.% eq. NaCl: Navarro-Ciurana et al., 2016a) brine with metals (Pb^{2+}, Zn^{2+}, Fe^{2+}) and Triassic sulfate.
(2) Fluid A: Percolated low temperature seawater (< 5 wt.% eq. NaCl: Navarro-Ciurana et al., 2016a).
(3) Organic compounds (e.j., hydrocarbons, dissolved metane).
(4) Mixing, **Fluid A > Fluid B**: equilibrated in temperature with time.
(5) Formation of pre-ore dolomitization (stratabound and patchy dolostones).
(6) Isothermal mixing, **Fluid B > Fluid A** equilibrated in temperature but not in salinity.
(7) Formation of ore sulfides by **TSR** reaction:

A- Slow growth formation of sulfides (well formed crystals): Fluid B with metals and sulfate interacted with organic compunds (metane).

$$2SO_4^{2-} + 2CH_4 + Pb^{2+} + Zn^{2+} = PbS + ZnS + 2CO_2 + 4H_2O$$

B- Fast growth formation of sulfides (botryodial morphologies):
Metal content of Fluid B decrases, consequently:

$$2H^+ + SO_4^{2-} + CH_4 = H_2S + CO_2 + 2H_2O$$

Posteriorly, metal content of Fluid B increases, consequently:

$$H_2S + Zn^{2+} = ZnS + 4H^+$$

Fig. 17. Idealized sketch of the pre-ore dolomitization stage and the Riópar Zn-(Fe-Pb) formations during Upper Cretaceous time, assuming a thermal gradient of 33 °C/km. Restitution according to cross section of Fig. 3. P: Paleozoic; Tr: Triassic clays and sandstones; Ji: Lower Jurassic dolostones; Jm: Middle Jurassic dolostones; Js_1: Puerto Lorente Fm; Js_2, Js_3, Ci_1: Sierra del Pozo Fm; Ci_2: Cerro Lobo Fm; Ci_3: Arroyo de los Anchos Fm; Ci_4: sandstones and clays of Utrillas facies; Ci_5: dolostones of Utrillas facies; Cs_1, Cs_2, Cs_3: Cenomanian-Turonian dolostones; Cs_4: Coniacian-Santonian limestones.

7.5. Mechanism(s) of sulfide deposition and metallogenetic model

Precipitation of base-metal sulfides at Riópar probably occurred with an effectively unlimited sulfur supply, as shown by the sulfur isotopic equilibrium between sphalerite and galena (Fig. 14). It is therefore a reasonable speculation that the low ore tonnage could have been caused by a low metal content in the fluid or by the low reductant agent content. As discussed above, a TSR is the most plausible sulfate reduction mechanism at Riópar. Organic matter and/or hydrocarbons could have been the sulfate reducing agents, triggering ore deposition when a metal-bearing fluid mixed with the H_2S-rich reservoir. Precipitation of sulfides in MVT deposits is widely accepted as the result of mixing of two fluids (e.g., Shelton et al., 1992; Kesler, 1996; Grandia et al., 2003a; Muchez et al., 2005). The model involves mixing of a metal-rich fluid (as chloride complexes) and a gas or/and a liquid reservoir containing reduced sulfur (e.g., Corbella et al., 2004; Leach et al., 2005). This conceptual model of ore formation is postulated for the world class Reocín MVT deposit (Basque-Cantabrian Basin; Velasco et al., 2003) and for the Mas de la Mina-Cedramán and Valdelinares Zn-Pb mineralization (Maestrat Basin; Grandia et al., 2003a), respectively. Other mechanisms of sulfide precipitation are possible: a local sulfate reduction, which involves the mixing of a fluid rich in sulfates and metals with a gas or/and a liquid containing a reducing agents (e.g., organic compounds; Anderson, 2008). At Riópar, based on microthermometrical data of fluid inclusions in dolomite and sphalerite, Navarro-Ciurana et al. (2016a) suggested that two fluids of contrasting salinities (Fluid A, < 5 wt% eq. NaCl; Fluid B, > 25 wt% eq. NaCl) but similar temperatures mixed at different fluid proportions.

No organic matter (bitumen) has been observed in the Upper Berriasian to Lower Valanginian age host rocks, but hydrocarbon inclusions are common in sphalerite crystals (Navarro-Ciurana et al., 2016a). Moreover, millimeter- to centimeter-scale lignite layers (Fig. 2) are found within the marl and limestone rhythmic sequence of the Cerro Lobo Fm (Upper Valanginian to Hauterivian). On the other hand, the intraclastic black pebbles ("cailloux noire") and ferruginous pisolitic limestones of the Arroyo de los Anchos Fm (Barremian-Aptian: Fig. 2) are characterized by a fetid odor, typical of hydrogen sulfide or sulfurous organic substances. Furthermore, different gas prospect projects have been developed in the Internal Prebetic Zone by BP and Repsol in the Neocomian to Barremian carbonatic sequence (Martínez del Olmo et al., 2013). Therefore, the presence of H_2S-bearing reservoirs in the region acting as chemical traps for the metals carried by hydrothermal fluids of basinal origin is plausible. Mixing between metal-bearing fluids and H_2S-rich reservoirs could result in relatively rapid sulfide precipitation under high supersaturation conditions; fine-grained and botryoidal sulfide crystal would then form (Anderson, 2008). However, if the gas reservoir was mainly composed of CH_4, reaction with sulfate in the ore solution via TSR would result in H_2S gas formation at a relatively slow rate, resulting in sulfide precipitation under low saturation degrees and leading to well-formed sulfide crystals (Anderson, 2008). In the Riópar area well-formed sulfide crystals is the most common texture, but botryoidal sphalerite morphologies are also recognized. This coexistence suggests an intermittent flow of the metal-bearing solution or a continuous flow with intermittent or variable metal content. If the metal amount decreased enough, the reaction of CH_4 with sulfate would generate a certain amount of H_2S gas. Therefore, with subsequent increases in the metal content in the hydrothermal system, the base metals would preferably react with H_2S gas producing fast growth morphologies (e.g., botryoidal sphalerite). This intermittent mechanism can explain the coexistence of slow and fast growth textures in the same deposit and in a restricted formation time period.

Geological, mineralogical and geochemical data point to a conceptual genetic model involving two fluids. A high salinity hydrothermal brine (average temperature of 220–230 °C: sphalerite Ga/Ge geothermometer), "Fluid B" of Navarro-Ciurana et al., 2016a, carrying both metals and sulfate (Triassic seawater or/and dissolution of evaporites), circulated through the Paleozoic basement, leaching base metals (Fig. 17-1). The other fluid, "Fluid A" of Navarro-Ciurana et al. (2016a), was of lower salinity and temperature and might be related to connate waters trapped within sediments of Mesozoic age (Fig. 17-2) containing organic rich compounds (e.g., hydrocarbons and CH_4 dissolved gas) (see Fig. 17-3). Therefore, the model proposed for the Riópar mineralization differs notably from the conceptual genetic scenarios of the Basque-Cantabrian and Maestrat MVT deposits (Velasco et al., 2003; Grandia et al., 2003a).

Mixing of both fluids at the ore deposition site occurred at different proportions during the dolomitization and mineralization stages. As heat conduction is faster than solute diffusion, and fluids of different salinity take time to homogenize, both fluids equilibrated in terms of temperature (150–250 °C: Navarro-Ciurana et al., 2016a) at the mineralization site but preserving batches of different salinity.

During pre-ore dolomitizing stage the hydrothermal system was dominated by the less saline fluid (connate waters) (Fluid A > Fluid B; Fig. 17-4) preventing sulfide precipitation because the lack of metals at this stage (Fig. 17-5; Navarro-Ciurana et al., 2016a). In a later stage, a flux increase of the high salinity metal-bearing fluid (basinal fluid), possibly due to a reactivation of the San Jorge fault, caused sulfide precipitation as it mixed with the low-salinity, hydrocarbon-rich reservoir (Fluid A < Fluid B; Fig. 17-6). Basinal fluid sulfate was then thermochemically reduced to H_2S by interaction with methane or other organic compounds at the depositional site, precipitating sulfide minerals (Fig. 17-7A). The coexistence of fast and slow growth textures in marcasite and sphalerite might be related to successive reactivations of the fault system structurally controlling the ores that took probably place during Upper Cretaceous to Tertiary times.

Previous to the botryoidal sphalerite precipitation, the ratio between metal content and sulfate of the high salinity fluid (Fluid B) would decrease, with the consequent H_2S gas formation, and accumulation, through CH_4-SO_4^{2-} reaction in the deposition site (Fig. 17-7B). A subsequent influx of fluid with a higher metal/sulfate ratio would thus prompt the precipitation of fast growth and botryoidal sphalerite textures from a direct reaction of Zn^{2+} and the H_2S accumulated (Fig. 17-7B). Furthermore, previously and posteriorly to sulfide mineral precipitation, a saddle dolomite gangue generation occurred, which is consistent with this intermittent contributions of metals during the ore-stage formation.

7.6. Exploration criteria

MVT deposits are characteristically distributed over hundreds of square kilometers (km^2) that define individual ore districts (Leach et al., 2010). For example in the Basque-Cantabrian Basin (~2500 km^2) around 40 deposits are recognized (Velasco et al., 1996; Grandia et al., 2003b). In contrast, the Riópar MVT mineralization is the only deposit that has been discovered and exploited in all of the Prebetic Zone so far. It may host many more, thus this area could be of interest for exploration.

Navarro-Ciurana et al., 2016c recognized a non-sulfide mineral occurrence not far from Riópar, which has never been described before in the literature. This new supergene mineralization, hosted within Barremian to Lower Aptian dolomitized carbonates is located in the westernmost part of the studied area, near Fuente de la Calentura (Fig. 4). It consists mainly of crusts of Fe oxi-hydroxides, which are similar to the supergenically altered uppermost parts of the San Jorge and San Agustín deposits. Although this new occurrence has not been further investigated yet, a corresponding deeper hypogene mineralization is to be expected.

As discussed above, the dolomitizing and mineralizing fluid in the study area mainly ascend along San Jorge fault, which continues to the SW with the Alto Guadalquivir fault (Fig. 1b). During the Upper Cretaceous, this fluid hydrothermally dolomitized the Upper Jurassic to

Lower Cretaceous carbonate sequence in the study area, which had previously been ascribed a Middle Jurassic age (Fernández-Gianotti et al., 2001). In addition, part of the dolostones that outcrop in the footwall block of the Alto Guadalquivir fault have also been interpreted as Middle Jurassic (i.e., García-Hernández et al., 2004). Therefore, is it possible that these dolostones are not of Middle Jurassic but of Upper Jurassic to Lower Cretaceous age? And, as these carbonates outcrop next to the Alto Guadalquivir-San Jorge fault, is it plausible that they have also been affected by hydrothermal fluids similar to those of the studied area? We think so and it is worth exploring.

Therefore, the vectors for the MVT exploration in the Prebetic Zone points towards the SW of the Riópar mines, in the area limited by Socovos and Alto Guadalquivir-San Jorge faults, towards the Fuente de la Calentura occurrence and in the vicinity of the Alto Guadalquivir fault. This area could contain hydrothermal dolomites, and as Navarro-Ciurana et al. (2016b) suggest, the C and O isotope signature of these dolomites may be a useful tool to reassess their origin. These dolomites are favorable potential hosts for economic Zn deposits.

8. Conclusions

The integration of geological and geochemical data presented here, with previously published data, allows us to draw the following conclusions regarding the ore controls, sulfur and metal sources, relative timing and the role of fluids during the ore formation at Riópar (Prebetic Zone, SE Spain). Ore controls are stratigraphic, lithologic and chemical for the stratabound pre-ore dolomitization, and tectonic for the pre-ore patchy dolomitization and the Zn-(Fe-Pb) ore stages. The distribution of Zn-(Fe-Pb) sulfide mineral occurrences suggests the San Jorge fault acted as the major conduit of the ore-bearing fluids from the source region (Paleozoic basement) to the deposition site (Upper Jurassic and Lower Cretaceous age dolomites). The fast flow along the fault prevented the complete cooling of the fluid from the reservoir (Ga/Ge geothermometer: 194–252 °C) to the precipitation site (isotope geothermometer 159 ± 15 °C). The $\delta^{34}S$ of sulfides (−7.5 to +3.5‰) is consistent with a thermochemical reduction of sulfate of Triassic age (seawater or/and dissolution of evaporites: $\delta^{34}S$ +12 to +16‰). Furthermore, the lead-isotope ratios ($^{206}Pb/^{204}Pb$ = 18.736–18.762; $^{207}Pb/^{204}Pb$ = 15.629–15.660; $^{208}Pb/^{204}Pb$ = 38.496–38.595) of galena suggest that Pb and metals are derived from continental crustal rocks, pointing to metal sources within the Paleozoic basement. Although, the precise age(s) of the ore is uncertain, a relative age of Upper Cretaceous to Tertiary is most likely for the dolomitization and mineralization. A mixing model involving of two fluids is postulated for the pre-ore dolomitization and sulfide mineralization. Fluid A (probably Cretaceous seawater), with organic rich compounds (e.g., hydrocarbons; methane), flowed through Mesozoic strata; it mixed with Fluid B (hydrothermal brine), containing metals and sulfate, after circulating through the Paleozoic basement. During the pre-ore dolomitizing stage the fluid phase was dominated by the diluted fluid (Fluid A > Fluid B) whereas in later fluid pulses, the mixing proportion of high salinity fluid increased (Fluid A < Fluid B) allowing sulfide mineral precipitation. In addition, in the Riópar area well formed (slow growth texture) and botryoidal (fast growth texture) sulfide morphologies coexist, suggesting different reaction pathways. When the organic reservoir (e.g., hydrocarbons and/or gas contained mainly CH_4) and metals were present, reaction with sulfate via TSR resulted in a relatively slow sulfide mineral precipitation; whereas when the amounts of metals was lower, reaction with CH_4 and sulfate resulted in spare H_2S gas that would be used up upon the arrival of a rich-metal batch a relatively fast growth sulfide mineral precipitation. Even though more work is needed, the principal vector for the MVT exploration in the Prebetic Zone points towards the SW of the Riópar ores, in the vicinity of the Alto Guadalquivir-San Jorge fault.

Acknowledgments

This research has been supported by the *Ministerio de Economía y Competitividad of Spain*, through the CGL2011-26488 project. The paper is part of the junior author's Geology thesis within the Geology PhD Program at *Universitat Autònoma de Barcelona* (MEE2011-0492). The authors would like to acknowledge Federico Ballesta (*Ciencia y Aventura*) for their support in the fieldwork. We also express our gratitude to Franco Pirajno, José María González Jiménez and two anonymous reviewers for comments that significantly improve the quality of the manuscript.

Appendix A. Supplementary data

Supplementary data associated with this article can be found, in the online version, at http://dx.doi.org/10.1016/j.oregeorev.2017.08.013.

References

Anderson, G.M., 2008. The mixing hypothesis and the origin of Mississippi Valley-type ore deposits. Econ. Geol. 103, 1683–1690. http://dx.doi.org/10.2113/gsecongeo.103.8.1683.

Arnorsson, S., 1984. Germanium in Icelandic geothermal Systems. Geochim. Cosmochim. Acta 48, 2489–2502. http://dx.doi.org/10.1016/0016-7037(84)90300-4.

Arribas, A.J., Tosdal, R.M., 1994. Isotopic composition of Pb in ore deposits of the Betic Cordillera, Spain: origin and relationship to other European deposits. Econ. Geol. 89, 1074–1903. http://dx.doi.org/10.2133/gsecongeo.89.5.1074.

Azéma, J., 1977. Étude géologique des zones externes des Cordilleres Bétiques aux confins des provinces d' Alicante et de Murcie (Espagne). Unpublished Ph.D. thesis, Pierre et Marie Curie, Paris VI, 393 pp.

Banks, C.J., Warburton, J., 1991. Mid-crustal detachment in the Betic system of southeast Spain. Tectonophysics 191, 275–289. http://dx.doi.org/10.1016/0040-1951(91)90062-W.

Barbero, L., López-Garrido, A.C., 2006. Mesozoic thermal history of the Prebetic continental margin (southern Spain): constraints from apatite fission-track analysis. Tectonophysics 422, 115–128. http://dx.doi.org/10.1016/j.tecto.2006.05.011.

Barton, P.B., Toulmin, P., 1966. Phase relations involving sphalerite in the Fe-Zn-S system. Econ. Geol. 61, 815–849. http://dx.doi.org/10.2113/gsecongeo.61.5.815.

Catanzaro, E.J., Murphy, T.J., Shields, W.R., Garner, E.L., 1968. Absolute isotopic abundance ratios of common, equal-atom, and radiogenic lead isotopic standards. J. Res. Nat. Bur. Stand. 72A, 261–267. http://dx.doi.org/10.6028/jres.072A.025.

Claypool, G.E., Holser, W.T., Kaplan, I.R., Sakai, H., Zak, I., 1980. The age curves of sulfur and oxygen isotopes in marine sulfate and their mutual interpretation. Chem. Geol. 28, 199–260. http://dx.doi.org/10.1016/0009-2541(80)90047-9.

Comas, M.C., Platt, J.P., Soto, J.I., Watts, A.B., 1999. The origin and history of the Alboran Basin, insights from ODP Leg 161 results (Western Mediterranean). In: Zahn, R., Comas, M.C., Klaus, A. (Eds.), Proceedings of the Ocean Drilling Program, Texas, Scientific Results, Collage Station 161, pp. 555–580.

Cooke, D.R., Bull, S.W., Large, R.R., McGoldrick, P.J., 2000. The importance of oxidized brines for the formation of Australian Proterozoic stratiform sediment-hosted Pb-Zn (sedex) deposits. Econ. Geol. 95, 1–18. http://dx.doi.org/10.2113/gsecongeo.95.1.1.

Corbella, M., Ayora, C., Cardellach, E., 2004. Hydrothermal mixing, carbonate dissolution and sulfide precipitation in Mississippi Valley-type deposits. Miner. Deposita 39, 344–357. http://dx.doi.org/10.1007/s00126-004-0412-5.

Czamanske, G.K., 1974. The FeS content of sphalerite along the chalcopyrite-pyrite-bornite sulfur fugacity buffer. Econ. Geol. 69, 1328–1334. http://dx.doi.org/10.2113/gsecongeo.69.8.1328.

De Botella y Hornos, 1868. Descripción geológica-minera de las provincias de Murcia y Albacete.

De la Escosura, L., 1845. De la mina de Zinc y fábricas de latón de S. Juan de Alcaráz junto a Riópar. Anales de Minas 3 198-155.

De Ruig, M.J., 1992. Tectono-sedimentary evolution of the Prebetic fold belt of Alicante (SE Spain). A study of stress fluctuations and foreland basin deformation. Unpublished Ph.D. thesis, Univ. Utrecht. 207 pp.

Dunnington, H.V., 1967. Aspects of diagenesis and shape change in stylolitic limestone reservoirs: 7th World Petroleum Congress, 2–9 April 1967, Mexico City, Mexico, 2, 339–352 pp.

Fenoll Hach-Alí, P., 1987. Los yacimientos de F-Pb-Zn-Ba del sector central de la Cordillera Bética. Univ. Granada.

Fernández-Gianotti, J., Perucha, M.A., Benito, M.I., Rodríguez-Estrella, T., Nozal, F., Gómez-Fernández, J.J., Meléndez, J.J., Aragón, R., Hornero, J., 2001. Mapa Geológico de España 1:50.000, hoja n° 866 (Yeste). I.G.M.E. Mem., 48 pp.

García-Hernández, M., López-Garrido, A.C., Vera, J.A., 2004. El Prebético del sector central y afloramientos más occidentales. In: Vera, J.A. (Ed.), Geología de España. Sociedad Geológica de España e Instituto Geológico de España, 363–372 pp.

García-Hernández, M., Lopz-Garrido, A.C., Rivas, P., Sanz de Galdeano, C., Vera, J.A., 1980. Mesozoic palaeogeographic evolution of the external zones of the Betic Cordillera. Geol. en Mijnb. 59, 155–168.

Grandia, F., 2000. Origin, evolution and age of the fluids related to Zn-Pb deposits in Cretaceous carbonates in the Maestrat Basin. Unpublished Ph.D. thesis, Univ.

Autònoma de Barcelona, 221 pp.
Grandia, F., Cardellach, E., Canals, À., 2001. Estudio petrográfico de las mineralizaciones de Zn-Pb de Riópar (Provincia de Albacete, España). Unpublished report.
Grandia, F., Cardellach, E., Canals, À., Banks, D.A., 2003a. Geochemistry of the fluids related to epigenetic carbonate-hosted Zn-Pb deposits in the Maestrat basin, Eastern Spain: fluid inclusion and isotope (Cl, C, O, S, Sr) evidence. Econ. Geol. 98, 933–954. http://dx.doi.org/10.2113/gsecongeo.98.5.933.
Grandia, F., Asmeromb, Y., Gettyc, S., Cardellacha, E., Canals, À., 2000. U-Pb dating of MVT ore-stage calcite: implications for fluid flow in a Mesozoic extensional basin from Iberian Peninsula. J. Geochem. Explor. 69–70, 377–380. http://dx.doi.org/10.1016/S0375-6742(00)00030-3.
Grandia, F., Canals, À., Cardellach, E., Banks, D.A., Perona, J., 2003b. Origin of ore-forming brines in sediment-hosted Zn-Pb deposits of the Basque-Cantabrian basin, Northern Spain. Econ. Geol. 98, 1397–1411. http://dx.doi.org/10.2113/gsecongeo.98.7.1397.
Helgeson, H.C., 1969. Thermodynamics of hydrothermal systems at elevated temperatures and pressures. Am. J. Sci. 267, 729–804. http://dx.doi.org/10.2475/ajs.267.7.729.
Kant, W., Warmada, W., Idrus, A., Setijadji, L.D., Watanabe, K., 2012. Ore mineralogy and mineral chemistry of pyrite, galena, and sphalerite at Soripesa prospect area, Sumbawa Island, Indonesia, SE Asian. J. Appl. Geol. 4, 1–14.
Kesler, S.E., 1996. Appalachian Mississippi valley-type deposits: paleoaquifers and brine provinces. In: Sangster, D.F. (Ed.), Carbonate Hosted Lead-zinc Deposits, Society of Economic Geologists Special Publication 4, 29–57.
Leach, D.L., Sangster, D.F., 1993. Mississippi Valley-type lead-zinc deposits. In: Kirkham, R.V., Sinclair, W.D., Thorpe, R.I., Duke, J.M. (Eds.), Mineral Deposits Modeling. Geological Association of Canada Special Paper, 289–314 pp.
Leach, D.L., Sangster, D.F., Kelley, K.D., Large, R.R., Garven, G., Allen, C.R., Gutzmer, J., Walters, S., 2005. Sediment-hosted lead-zinc deposits: a global perspective. Economic Geology 100th Anniversary Volume, 561–608 pp.
Leach, D.L., Taylor, R.D., Fey, D.L., Diehl, S.F., Saltus, R.W., 2010. A deposit model for Mississippi valley-type lead-zinc ores. Scientific Investigations Report Geological Survey, 64 pp.
Lind, I.L., 1993. Stylolites in chalk from Leg 130, Ontong Java Plateau, in Proceedings of the Ocean Drilling Program, Scientific results, Volume 130: College Station, Texas, Ocean Drilling Program, 445–451 pp.
Machel, H.G., Krouse, H., Sassen, R., 1995. Products and distinguishing criteria of bacterial and thermochemical sulfate reduction. Appl. Geochem. 10, 373–389. http://dx.doi.org/10.1016/0883-2927(95)00008-8.
Martínez del Olmo, W., Martín, D., Motis, K., 2013. El Cretácico del Prebético Interno en la región de Moratalla (Murcia, SE de España). Rev. Soc. Geol. Esp. 12, 13–22.
Michel, B., 1974. Contributions a l'étude des mineralizations plombozincifères dans le Crétacé Inferieur du Maestrazgo. Unpublished Ph.D. thesis, Universite de Nancy, 178 pp.
Möller, P., 1985. Development and application of the Ga/Ge-Geothermometer for sphalerite from sediment hosted deposits. In: Germann, K. (Ed.), Geochemical aspects for Ore Formation in Recent and Fossil Sedimentary Environments, 15–30 pp.
Möller, P., 1987. Correlation of homogenization temperatures of accessory minerals from sphalerite-bearing deposits and Ga/Ge model temperatures. Chem. Geol. 61, 153–159. http://dx.doi.org/10.1016/0009-2541(87)90035-0.
Mountjoy, E.W., Amthor, J.E., 1994. Has burial dolomitization come of age? Some answers from the Western Canada Sedimentary Basin. Int. Assoc. Sedimentol. Spec. Publ. 21, 203–229.
Muchez, P., Heijlen, W., Banks, D., Blundell, D., Boni, M., Grandia, F., 2005. Extensional tectonics and the timing and formation of basin-hosted deposits in Europe. Ore Geol. Rev. 27, 241–267. http://dx.doi.org/10.1016/j.oregeorev.2005.07.013.
Murowchick, J.B., Barnes, H.L., 1986. Marcasite precipitation from hydrothermal solutions. Geochim. Cosmochim. Acta 50, 2615–2629. http://dx.doi.org/10.1016/0016-7037(86)90214-0.
Navarro-Ciurana, D., Corbella, M., Cardellach, E., Vindel, E., Gómez-Gras, D., Griera, A., 2016a. Petrography and geochemistry of fault-controlled hydrothermal dolomites in the Riópar area (Prebetic Zone, SE Spain). Mar. Pet. Geol. 71, 310–328. http://dx.doi.org/10.1016/j.marpetgeo.2016.01.005.
Navarro-Ciurana, D., Griera, A., Gómez-Gras, D., Cardellach, E., Vindel, E., Corbella, M., 2016b. Dolostone origin in the Riópar area (SE Spain): implications on the geology of the Prebetic Zone. Geo-Temas (accepted).
Navarro-Ciurana, D., Campos-Quispe, L.A., Cardellach, E., Vindel, E., Gómez-Gras, D., Griera, A., Corbella, M., 2016c. Mineralogical and geochemical characterization of the Riópar non-sulfide Zn-(Fe-Pb) deposits (Prebetic Zone, SE Spain). Ore Geol. Rev. 79, 515–532. http://dx.doi.org/10.1016/j.oregeorev.2016.05.023.
Nicolaides, S., Wallace, M.W., 1997. Pressure dissolution and cementation in an Oligo-Miocene non-tropical limestone (Clifton Formation), Otway Basin, Australia. In: James, N.P.C., Clarke, J.A.D. (Eds.), Cool-water carbonates: SEPM (Society for Sedimentary Geology) Special Publication 56, 249–261.
Ohmoto, H., Rye, R.O., 1979. Isotopes of sulfur and carbon. In: Barnes, H.L. (Ed.), Geochemistry of Hydrothermal Ore Deposits, 2nd ed. Wiley, New York, pp. 509–567.
Ortí, F., Pérez-López, A., García-Veigas, J., Rosell, L., Cendón, D.I., Pérez-Valera, F., 2014. Sulfate isotope compositions ($\delta^{34}S$, $\delta^{18}O$) and strontium isotopic ratios ($^{87}Sr/^{86}Sr$) of Triassic evaporites in the Betic Cordillera (SE Spain). Rev. Soc. Geol. Esp. 27, 79–89.
Paytan, A., Kastner, M., Campbell, D., Thiemens, M.H., 2004. Seawater sulfur isotope fluctuations in the Cretaceous. Science 304, 1663–1665. http://dx.doi.org/10.1126/science.1095258.
Pellicio, R.P., 1845. Minas de Zinc de San Juan de Alcaraz en la provincia de Albacete. Boletín Oficial de Minas 19, 323–326.
Pérez-Valera, L.A., Sánchez-Gómez, M., Fernández-Soler, J.M., Pérez-Valera, F., Azor, A., 2010. Diques de lamproítas a lo largo de la falla de Socovos (Béticas orientales). Geogaceta 48, 151–154.
Perona, J., Cardellach, E., Canals, À., 2007. Origin of diapirrelated Zn-Pb deposits in the Basque-Cantabrian Basin (Northern Spain). In: Andrew, C.J. et al. (Eds.), Proceedings of the ninth biennial SGA meeting, Dublin. Irish Association for Economic Geology, Digging Deeper 2, 1303–1306.
Piqué, À., Canals, À., Disnar, J.-R., Grandia, F., 2009. In situ thermochemical sulfate reduction during ore formation at the Itxaspe Zn-(Pb) MVT occurrence (Basque-Cantabrian basin, NE Spain). Geol. Acta 7, 431–449.
Plumlee, G.S., Leach, D.L., Hofstra, A.H., Landis, G.P., Rowan, E.L., Viets, J.G., 1994. Chemical reaction path modeling type Pb-Zn deposits of the of ore deposition in Mississippi Valley Ozark Region, U.S. Midcontinent. Econ. Geol. 89, 1361–1383. http://dx.doi.org/10.2113/gsecongeo.89.6.1361.
Rodríguez-Estrella, T., 1979. Geología e Hidrogeología del Sector de Alcaraz – Liétor – Yeste (Provincia de Albacete). Instituto Geológico i Minero de España 97, 566 pp.
Sanz de Galdeano, C., 1990. Geologic evolution of the Betic Cordilleras in the Western Mediterranean, Miocene to the present. Tectonophysics 172, 107–119. http://dx.doi.org/10.1016/0040-1951(90)90062-D.
Scott, S.D., 1974. Experimental methods in sulfide synthesis. In: Ribbe, P.H. (Ed.), Sulfide mineralogy. Mineralogical Society of America, Short Course Notes 1, Sl–S38.
Scott, S.D., 1983. Chemical behavior of sphalerite and arsenopyrite in hydrothermal and metamorphic environments. Mineral. Mag. 47, 427–435. http://dx.doi.org/10.1180/minmag.1983.047.345.03.
Shelton, K.L., Bauer, R.M., Gregg, J.M., 1992. Fluid-inclusion studies of regionally extensive epigenetic dolomites, Bonneterre Dolomite (Cambrian), southeast Missouri: evidence of multiple fluids during dolomitization and lead-zinc mineralization. Geol. Soc. Am. Bull. 104, 675–683. http://dx.doi.org/10.1120/0016-7606(1992)104<0675:FISORE>2.3.CO;2.
Simon, S., Canals, À., Grandia, F., Cardellach, E., 1999. Estudio isotópico y de inclusiones fluidas en depósitos de calcita y dolomita del sector oeste del Anticlinal de Bilbao y su relación con las mineralizaciones de Fe-Zn-Pb. Boletín Sociedad Española de Mineralogía 22, 55–71.
Symons, D.T.A., Lewchuk, M.T., Kawasaki, K., Velasco, F., Leach, D.L., 2009. The Reocín zinc-lead deposit, Spain: paleomagnetic dating of a late Tertiary ore body. Miner. Deposita 44, 867–880. http://dx.doi.org/10.1007/s00126-009-0253-3.
Stacey, J.S., Kramers, J.D., 1975. Approximation of terrestrial lead isotope evolution by a two-stage model. Earth Planet. Sci. Lett. 26 (2), 207–221. http://dx.doi.org/10.1016/0012-821X(75)90088-6.
Tritlla, J., Solé, J., 1999. A newly dated Cretaceous hydrothermal event in the Iberian Ranges (Eastern Spain) and its significance within the Mesozoic thermal history in the Iberian Peninsula. Ore Geol. Rev. 15, 243–259. http://dx.doi.org/10.1016/S0169-1368(99)00009-8.
Urbano-Vicente, R., 1972. Exploración Minera Internacional (España), S.A. Unpublished report.
Velasco, F., Pesquera, A., Herrero, J.M., 1996. Lead isotope study of Zn-Pb ore deposits associated with the Basque-Cantabrian basin and Paleozoic basement, northern Spain. Miner. Deposita 31, 84–92. http://dx.doi.org/10.1007/BF00225398.
Velasco, F., Herrero, J.M., Iñaki, Y., Alonso, J.A., Seeblod, I., Leach, D., 2003. Geology and Geochemistry of the Reocín Zinc-Lead deposit, Basque-Cantabrian Basin, Northern Spain. Econ. Geol. 98, 1371–1396. http://dx.doi.org/10.2113/gsecongeo.98.7.1371.
Velasco, F., Alonso, J.A., Cueto, J., Herrero, J.M., Muñoz, F., Seebold, I., Yusta, I., 2000. Relación entre dolomitización y mineralización en el yacimiento de Zn-Pb de Reocín, Cuenca Vasco-Cantábrica, España. Cuadernos de Laboratorio Xeológico de Laxe 25, 135–137.
Vera, J.A., 2001. Evolution of the South Iberian Continental Margin. In: Ziegler, P.A., Cavazza, W., Robertson, A.H.F., Crasquin-Soleau, S. (Eds.), Peri-Tethyan rift/wrench basins and passive margins. Mém. Mus. Natl. Hist. Nat. 186, 109–143.
Vera, J.A., Arias, C., García-Hernández, M., López-Garrido, A.C., Martín-Algarra, A., Martín-Chivelet, J., Molina, J.M., Rivas, P., Ruiz-Ortiz, P.A., Sanz de Galdeano, C., Vilas, L., 2004. Las zonas externas béticas y el paelomargen sudibérico. In: Vera, J.A. (Ed.), Geología de España. Sociedad Geológica de España e Instituto Geológico de España, pp. 354–360.
Vilas, L., Dabrio, C., Peláez, J.R., García-Hernández, M., 2001. Dominios sedimentarios generados durante el periodo extensional Cretácico inferior entre Cazorla y Hellín (Béticas Externas). Su implicación en la estructural actual. Rev. Soc. Geol. Esp. 14, 113–122.
Zartman, R.E., Doe, B.R., 1981. Plumbotectonics – the model. Tectonophysics 75, 135–162. http://dx.doi.org/10.1016/0040-1951(81)90213-4.